Astron. Astrophys. 332, 1099–1122 (1998)

ASTRONOMY AND ASTROPHYSICS

Chemical reactions in protoplanetary accretion disks

IV. Multicomponent dust mixture

H.-P. Gail

Institut für Theoretische Astrophysik, Universität Heidelberg, Tiergartenstraße 15, D-69121 Heidelberg, Germany (gail@ita.uni-heidelberg.de)

Received 24 October 1997 / Accepted 2 January 1998

Abstract. We consider the different major components of the dust mixture in protostellar accretion disks and the development of their structure and chemical composition as the disk material slowly migrates inwards during the viscous phase of the disk evolution. It is shown that the amorphous structure of the dust grains from the parent molecular cloud is converted by annealing at about 800 K into a well ordered crystalline lattice structure accompanied by a chemical differentiation by solid state diffusion processes. The chemical composition of the abundant refractory dust components formed from silicon, magnesium, iron, aluminium, and calcium is discussed on the basis of chemical equilibrium considerations. Convenient approximations for calculating the equilibrium abundance of the major dust components are derived. These are used to calculate a self consistent model for a stationary accretion disk around a one solar mass protosun in the one zone approximation and to derive the radial variation of the abundance of the different dust species. The model takes properly into account the strong coupling between disk structure, opacity, and the chemical composition and abundance of the major dust species, i.e. amorphous silicates in the cool parts of the disk, and olivine, orthopyroxene, iron, and aluminium compounds in the warm parts.

Key words: accretion, accretion disks – molecular processes – solar system: formation – dust, extinction

1. Introduction

All present theories of the origin of the Solar System require the existence of an accretion disk around the protosun. The disk results from infall of matter from a slowly rotating molecular cloud core. After an initial phase of build up of the disk of duration of roughly 10^5 yrs and a subsequent viscous phase of a few 10^5 yrs duration where the protostar acquires most of its mass by accretion from the disk there follows the clearing phase when infall from the parent molecular cloud has nearly ceased. It is believed that formation of a planetary system starts at the end of the viscous phase. The disk material in this stage of the evolution of the protoplanetary accretion disk is more or less unprocessed material from the parent molecular cloud which landed at large distances (beyond ≈ 30 AU) from the protosun on the disk (e.g. Cassen 1994) without being substantially modified during the passage of the accretion shock standing on the disk surface. All material which initially entered the disk close to the star, which has been processed there by strong heating, and some fraction of which has been transported by viscous transport processes out to large distances during the early evolution of the accretion disk, has been transported inwards during the late evolution of the disk and is incorporated into the protosun at the time of the onset of planetary formation.

As the dust material with the composition and structure as inherited from the molecular cloud during the disk accretion process slowly spirals inwards towards the protosun it enters disk regions of progressively higher temperatures. At sufficiently high temperatures energetic lattice vibrational states become populated by thermal excitation and less strongly bound atoms or groups of atoms start to diffuse around within the lattice. The resulting conversion of the amorphous structure of interstellar dust grains into an ordered lattice structure is accompanied by a strong modification of the extinction properties of the disk material. This annealing process and its consequences for the disk structure are discussed in this paper.

The dust material entering the disk from the parent molecular cloud is a mixture of many different solid condensates with quite different chemical compositions (cf. Pollak et al. 1994) originating from very different sources like circumstellar shells of late type giant and supergiant stars or from the ejecta of novae and supernovae. Due to the large variations in the formation conditions of the dust and the element abundances in the sources the composition of the dust mixture entering the protoplanetary accretion disk does not correspond to any mixture which can be formed in a single condensation process in an environment with a mixture of elements corresponding to Solar System element abundances. Such a mixture is chemically only metastable in the sense that at low temperatures (up to several 100 K) the dust material does not participate in chemical reactions which changes the amount of condensed material and the chemical composition of the solids. Such reactions are kinetically forbidden at low temperatures due to high activation energy barriers. At elevated temperatures, however, chemical reactions between solids and the gas phase species and (or) vapourisation of the solids be-

Send offprint requests to: H.-P. Gail

Table 1. Abundant dust species in the protoplanetary accretion disk, the fraction of the abundant elements condensed in the dust species, the stoichiometric coefficient x for the silicates, and their resp. melting temperatures

Name	Composition	Fractional abundance							Melting
		Mg	Fe	Si	S	C	O	x	[K]
Olivine	$Mg_xFe_{2-x}SiO_4$	0.83	0.42	0.63				1.4	2180
Orthopyroxene	$Mg_xFe_{1-x}SiO_3$	0.17	0.09	0.27				0.7	1850
Quartz	SiO_2			0.10					1996
Metallic iron	Fe		0.1						1811
Troilite	FeS		0.39		0.75				1460
Kerogen	CHON					0.55			

comes possible. In the warm inner parts of the accretion disk the initial dust mixture then starts to be chemically processed into a mixture of condensates corresponding to that mixture which corresponds to a chemical equilibrium state compatible with the pressure and temperature conditions encountered in the protoplanetary disk, and to the specific element mixture which results from equilibrating all compositional differences in the initial mixture.

Some processes which may be responsible for the destruction of the dust at elevated temperatures have been discussed in Duschl et al. (1996). In this paper we consider the multicomponent mixture of several kinds of dust species which can be expected to be formed in the inner parts of the protoplanetary disk in a state of thermodynamic equilibrium from the initial dust mixture of the molecular cloud. The varying composition of the matter in the Solar Nebula by the appearance and disappearance of different condensates from the most abundant elements with changing temperature has been studied several times by applying the concepts of equilibrium thermodynamics (e.g. Grossman 1972, Lattimer et al. 1978, Saxena & Eriksson 1986, Sharp & Huebner 1990). This paper follows to some extent the concepts of such studies, but we prefer to derive explicit expressions for the equilibrium abundance of the various possible condensates since it is convenient to use such expressions in model calculations for the structure of protoplanetary accretion disks. Especially we broadly discuss which type of dust materials formed from the elements O, Si, Mg, and Fe are the thermodynamically stable dust materials in an element mixture with the specific abundances as observed for the Solar System. These dust materials are of special importance since they represent the main sources of opacity in the disk material in the region of their existence and, thus, are crucial for the structure of the disk. The same holds for solid calcium and aluminium compounds which are stable up to quite high temperatures and are the main opacity sources of the disk material in some inner part of the protoplanetary accretion disk. We discuss in this paper which type of condensate can be expected to be present in the inner part of the disk where aluminium compounds are the dominating opacity sources.

The results of these calculations then are used to calculate a model for a stationary protoplanetary accretion disk in the one zone approximation which self consistently yields the disk structure and the chemical composition of the dust mixture in the warm inner parts of the accretion disk .

2. Initial composition of the dust mixture

The question of which types of dust formed from the most abundant dust forming elements, i.e., formed from the elements C, N, O, Mg, Si, S and Fe, can be expected to exist in molecular cloud cores and in the cool outer parts of a protoplanetary accretion disk has thoroughly been discussed by Pollak et al. (1994). They arrived at the conclusion that in the outer parts of the disk there exists a multicomponent mixture of several kinds of dust species, which is dominated most likely by the following few species:

- $Mg_xFe_{2-x}SiO_4$ (Olivine)
- $Mg_xFe_{1-x}SiO_3$ (Orthopyroxene)
- SiO_2 (Quartz)
- Fe (metallic iron)
- FeS (Troilite)
- CHON-Material (Kerogen).

Table 1 shows the best estimate of Pollak et al. (1994) for the fraction of the key elements Mg, Fe, Si, and S bound into these dust materials: The elements Mg, Fe, and Si are assumed to be completely condensed into this dust mixture while for S some fraction remains in the gas phas. The carbon is assumed to form a complex organic material containing considerable portions of H, N, and O besides the carbon. The numbers in Tab. 1 result from a critical discussion and evaluation of the observational material and probably represent the most reliable model for the composition of the dust material in molecular cloud cores and in protostellar disks which can presently be derived. We base our considerations in this paper with respect to the Mg-Fe-Si dust components on precisely this model. We shall call this the P94-mixture.

The P94 model for the dust composition is quite different from models for the interstellar dust composition, as for instance the widely used Mathis-Rumpl-Norsieck (1977) model or the model proposed by Li & Greenberg (1997). Especially the assumption of an iron and a troilite component is unusual. It is motivated by results of thermochemical equilibrium calculations (e.g. Grossman 1972, Lattimer et al. 1978, Prinn & Fegley

1989) and the existence of such grains in primitive meteorites. The recent detection of iron and troilite inclusions in glassy silicate grains of presumably interstellar origin (Bradley 1994, cf. also the discussion in Martin 1995, Goodman & Whittet 1995) lends some support to the assumptions of the P94 model. Also the models for the composition of interstellar dust discussed by Mathis (1996) shows for instance iron grains to be a possible component of the interstellar dust mixture.

Throughout the protostellar accretion disk, these dust components are in the solid state (cf. Tab. 1 and Fig. 3) because the upper limit of stability under protoplanetary disk conditions of all these dust components turns out to be well below their respective melting points.

The dust formed from the group of elements O, Mg, Fe, Si, and C is the main source of opacity in the protoplanetary accretion disk and, by this, determines the structure and time evolution of that part of the accretion disk where the disk is cool enough for these dust components to exist. From studies of primitive meteorites it is known that additional minor dust components formed from such elements existed in the protoplanetary disk (e.g. Sears & Dodd 1988), but they cannot be of substantial importance, neither for the disk structure and evolution nor for the chemistry of the abundant elements. Such minor dust components formed from the abundant elements O, Mg, Fe, Si, and C are neglected in the P94 dust model and so we will do.

The dominating dust components are not the most stable dust species existing at high temperatures. Compounds of the less abundant elements Al and Ca, for instance, can survive even if heated up to much higher temperatures than the Mg-Fe-Si-compounds. Dust species formed from these elements, especially corundum, then become the dominant opacity sources in part of the protoplanetary disk close to the protostar where the disk is too hot for the silicates to exist. From analysis of abundances ratios for oxygen and aluminium isotopes in meteoritic material it is known that corundum (Al_2O_3) and spinel ($MgAl_2O_4$) grains of definitely circumstellar origin have been present in the protoplanetary disk material (e.g. Hutcheon et al. 1994, Huss et al. 1994, Nittler et al. 1994). Thus, at least part of the total aluminium content of the infalling material from the parent molecular cloud entered the protoplanetary disk as a separate dust component. The aluminium dust components are considered in some detail in Sect. 5.

Compounds of the less abundant elements Ti and Zr may exist at temperatures above the stability limit of the silicates and at even much higher temperatures than the aluminium-calcium compounds. Their abundance is too low as that they can become important sources of dust opacity. We do not consider such dust species in this paper, though they may be important as seed nuclei for dust condensation.

3. Annealing and diffusion I

It is generally believed that the internal microstructure of the lattice of interstellar and molecular cloud dust particles to a large extent is amorphous (cf. the review by Dorschner & Henning 1995). The dust within the protoplanetary disk is of precisely such an origin. It has fallen during the collapse phase from the molecular cloud onto the accretion disk. During the viscous stage of the protoplanetary disk the central protosun has already grown to nearly its final mass by accreting most of the mass contained in the disk. The remaining material within the accretion disk in this phase of its evolution essentially consists of material from the parent molecular cloud which most likely has landed on the disk at rather large distances ($\approx 10 \ldots 100$ AU) from the protostar (Cassen 1994). The infalling cloud material prior to its mixing with previously accreted disk matter passes through an accretion shock standing on both sides of the disk surface. In the outer parts of the accretion disk the strength of this shock is not particularly high and the dust component is not strongly heated or even destroyed during its passage through the shock (e.g. Lunine et al. 1991, Neufeld & Hollenbach 1994, Ruzmaikina & Ip 1994). Only ice coatings on the grains are vapourised, but in the outer parts of the disk at distances of $\approx$ 7 AU and more they are formed anewed when the grains and the gas cool behind the shock. The dust component of the disk matter during the viscous stage of disk evolution, thus, is expected to be almost unprocessed dust from the parent molecular cloud.

The inwards transport of matter during the viscous evolution of the disk carries the dust particles slowly into the hot central parts of the accretion disk where the dust ultimately is destroyed either by thermal decomposition or by chemical surface reactions at temperatures above 1 000 K for the carbonaceous dust component (Finocchi et al. 1997) and above 1 500 K for the silicate dust component (e.g. Duschl et al. 1996). At a somewhat lower temperature the dust already is subject to the process of annealing (Lenzuni et al. 1995, Duschl et al. 1996). At elevated temperature the lattice vibrations in the dust become sufficiently excited that activation energy barriers can be overcome such that atoms or groups of atoms may change their position or their orientation within the lattice. The atoms in the amorphous dust material then start to rearrange and to migrate into energetically more favourable positions or orientations within the lattice, where they are more tightly bound and, then, become less mobile. By this process the dust material gradually develops some kind of local order and slowly changes its lattice structure from the strongly disordered structure of an amorphous material to the locally ordered structure of a microcrystalline material. If the amorphous dust grains contain a significant fraction of impurity elements within their lattice, for instance Al and Ca replacing some of the kations or anions in the olivine lattice, then the annealing of lattice defects is accompanied by chemical fractionation within the grain. The impurities are gathered in separate inclusions or migrate to the grains surface. If annealing lasts sufficiently long even complete crystallisation of the previously amorphous grains may occur.

3.1. Silicate grains

The basic microscopic processes responsible for annealing are diffusion of vacancies and interstitials, and self-diffusion. For the purpose of a rough estimation these processes can be approx-

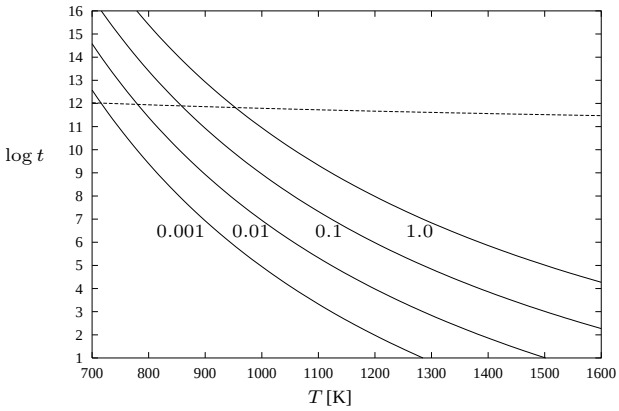

Fig. 1. Time scale t (in s) for solid state diffusion at temperature T within silicate dust particles of the indicated size (in μm). The dashed line shows the characteristic timescale τ_T for temperature changes in the accretion disk given by Eq. (68).

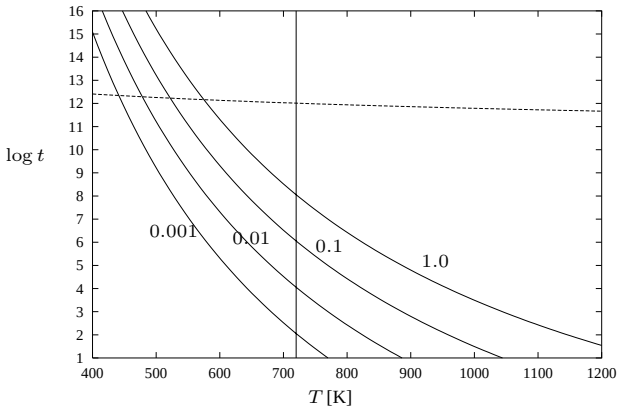

Fig. 2. Time scale t (in s) for solid state diffusion at temperature T of sulphur atoms within iron particles of the indicated size (in μm). The vertical line shows the limit temperature for the conversion of Fe into FeS in the disk model. The dashed line shows the characteristic timescale τ_T for temperature changes in the accretion disk given by Eq. (68).

imated by a 3D random walk on a cubic lattice. The diffusion coefficient in this case is

$$D = \frac{1}{3} a^2 \nu \mathrm{e}^{-E_a/kT} \tag{1}$$

(e.g. Dekker 1963). a is the average step length, ν is the number of attempts per unit time for hopping to a neighbouring lattice site and E_a is the activation energy. The characteristic activation energy for silicate materials has been estimated by Lenzuni et al. (1995) and Duschl et al. (1996) to be $E_a/k = 41\,000\,\mathrm{K}$ based on the annealing experiment of Nuth & Donn (1982) for condensates from magnesium-silicate smokes and assuming the characteristic frequency ν to equal the average vibrational frequency $\nu = 2\,10^{13}\,\mathrm{s}^{-1}$ of the SiO_4 tetrahedron. Essentially the same E_a results if one uses the Debye temperature $\Theta_D = 763\,\mathrm{K}$ for Mg_2SiO_4 (Kuskov & Galimzyanov 1986) for the determination of the characteristic frequency ν. The characteristic length a is estimated from the volume V of the basic molecule forming the lattice:

$$V = \frac{Am}{\rho} = a^3 \,. \tag{2}$$

$A = 140.7$ is the molecular weight of Mg_2SiO_4, m the atomic mass unit and $\rho = 3.21\,\mathrm{g/cm^3}$ the mass density of Mg_2SiO_4. We obtain for the coefficient of solid state diffusion within the silicate

$$D = 1.2\,10^{-2}\,\mathrm{e}^{-41\,000\,\mathrm{K}/T}\,[\mathrm{cm^2/s}]\,. \tag{3}$$

In a 3D random walk the average rms displacement d^2 within time t is given by

$$d^2 = 3 \cdot 2Dt\,. \tag{4}$$

Fig. 1 shows the typical time t required for a single atom to walk over some prescribed distance d. This may be identified with the time required for annealing the amorphous structure of unprocessed grains from the parent molecular cloud and to form at least a local crystal structure extending over regions of size d. We arbitrarily assume that diffusion over a distance of $d = 0.01\,\mu$m is required to convert the amorphous dust material into a locally ordered structure with (poly)crystalline properties. The time required for this has to be compared with the duration of the viscous stage of disk evolution which lasts for roughly $10^5 \ldots 10^6$ yrs. From Fig. 1 we infer that at temperatures above $\approx 800\,\mathrm{K}$ in the midplane of the disk the grains loose their amorphous structure by local rearrangement and gain an ordered lattice structure. We also can compare the diffusion timescale with the characteristic timescale τ_T for changes of the temperature in the frame of a gas parcel drifting towards the star, which is shown as a dashed line in Fig. 1. This also yields a limit temperature of $\approx 800\,\mathrm{K}$ above which the amorphous silicate dust material is converted into a crystalline one. The same conclusion has been arrived at in Duschl et al. (1996) by a slightly different argument. A laboratory experiment with striated orthopyroxene showed annealing of the structure by heating for one week to 1 100 K (Ashworth et al. 1984), roughly consistent with our estimation of diffusion timescales.

This annealing of any amorphous structure of the grains inherited from their circumstellar birth conditions allows to apply thermochemical data measured in the laboratory for crystalline materials to dust materials in protoplanetary disks, if one calculates dust compositions, vapourisation temperatures etc. It also requires to use data for *crystalline* dust materials in calculating the opacity in regions where the dust is heated to temperatures $\gtrsim 800\,\mathrm{K}$. This is discussed in detail within the context of model calculations in Sect. 7.

3.2. Iron grains

Besides silicate grains, iron metal grains are likely to exist in the accretion disk. For iron the measured value (by radioactive tracer diffusion) of the coefficient of self-diffusion is

$$D = 5.4 \cdot\ \mathrm{e}^{-30\,000\,\mathrm{K}/T}\,[\mathrm{cm^2/s}]\,. \tag{5}$$

(Weast 1981). The diffusion timescale for iron grains at a temperature of 1 000 K is approximately 10^{-8}-times shorter than the diffusion timescale for the silicates. Any possible amorphous structure of the iron, therefore, is removed already at rather low temperatures. An inspection of Fig. 2 shows that at temperatures above ≈ 500 K iron grains should develop at least locally a well ordered structure and above ≈ 600 K even the biggest grains of interstellar origin had enough time to rearrange into a well ordered lattice structure extending over the whole grain.

Many other abundant possible impurity atoms have diffusion coefficients with a very similar activation energy and frequency factor, for instance the metals Ni and Mn or the nonmetals S and P (Weast 1981). They can easely move around within the lattice which means that only components which are easely soluble in the iron metal remain inside the iron grains (Ni for instance, which then forms separate Ni-Fe crystals; this process has been studied in a computer simulation by Willis & Goldstein 1981) while non soluble elements most likely are driven out of the lattice and assemble at the surface of the grains from which they are lost to the gas phase. One can expect, thus, that iron grains in the warm part of an accretion disk are rather clean metal clusters.

The ease with which certain atoms may diffuse through the iron during the long period of time available as the grains slowly migrate inwards is especially important for the sulphur since at low temperature part of the iron forms FeS (see Sect. 4.3). The diffusion coefficient of S atoms in iron metal is

$$D = 1.7 \cdot \ \mathrm{e}^{-27\,000\,\mathrm{K}/T} \ [\mathrm{cm}^2/\mathrm{s}] \,. \tag{6}$$

(Weast 1981). The resulting characteristic diffusion timescale is shown in Fig. 2. The timescale at the stability limit of FeS is short enough even for micron sized grains that sulphur atoms may diffuse into or out of iron grains in order that the conversion of FeS to Fe or vice versa is possible.

3.3. Carbonaceous grains

Annealing of an amorphous structure is not possible for the carbonaceous dust component since this requires breaking of the strong C-C-bonds. The coefficient of self-diffusion for C in carbon is

$$D = 5 \cdot \mathrm{e}^{-82\,000\,\mathrm{K}/T} \ [\mathrm{cm}^2/\mathrm{s}] \tag{7}$$

(Weast 1981). Diffusion time scales at 1 000 K then are roughly 15 orders of magnitude longer than for silicates. Annealing of interlayer bonds from partially ordered carbon, however, is possible at medium temperatures. After processing a carbonaceous material to a temperature $\gtrsim 720$ K such bonds are essentially removed (Rietmeijer & Mackinnon 1985).

4. Equilibrium chemistry of the Mg-Fe-complex

The possible condensates formed from the elements Mg, Fe, and Si are only stable for temperatures where (i) H is completely associated to H_2, (ii) carbon not bound into carbon dust has formed CO and is completely locked up in this molecule, (iii) gas phase silicon is completely bound in the SiO molecule, and (iv) the remaining fraction of gas phase oxygen not bound in SiO or CO has formed H_2O molecules. The metals Fe and Mg are present as free atoms in the gas phase and nitrogen is completely bound in N_2. A lot of much less abundant additional molecular species of these elements, and atoms or molecules of the less abundant elements exist in the gas phase, but these are of no interest in the present context. At temperatures below $\approx 1\,000$ K when Si, Mg, and Fe are condensed into solids the SiO and CO are converted into SiO_2 and CO_2, respectively, and the metal atoms form hydroxides, but this not important for our calculations.

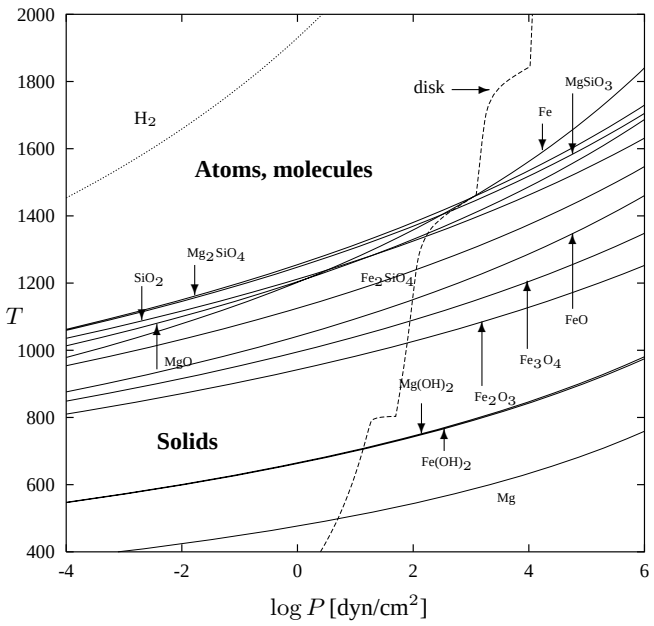

Fig. 3. Limit curves for the formation of refractory condensates of the abundant elements Mg, Fe, and Si from atoms or molecules *from the gas phase*. The dashed line shows the P-T stratification in the central plane of a protoplanetary disk model. The upper and lower inflections in this line correspond to the stability limits of corundum and olivine, respectively. The dotted line shows the limit curve for H_2 dissociation for comparison

In the following we consider the chemical equilibrium between a gas phase which is essentially composed of H_2, He, H_2O, CO, SiO, Fe, and Mg and the possible condensates which may be formed from these elements.

4.1. Pure metals

Let P denote the pressure of the gas phase and let P_{H} be the fictitious pressure of all hydrogen nuclei if they were present as free particles. If the hydrogen is completely associated to H_2 we have

$$P_{\mathrm{H}} = \frac{2P}{1 + 2\epsilon_{\mathrm{He}}} \,. \tag{8}$$

ϵ_{He} is the abundance of He (relative to H). Consider the condensation of metallic iron from the gas phase and let f be the

fraction of the totally available iron condensed into solid iron particles. If Fe is not bound into any other condensate the fraction $1-f$ of the Fe remains in the gas phase. Its partial pressure then is

$$p_{\rm Fe} = (1-f)\,\frac{2\epsilon_{\rm Fe}}{1+2\epsilon_{\rm He}}P\,. \tag{9}$$

In order that the condensed iron metal and the free iron atoms in the gas phase are in a state of thermodynamic equilibrium, the partial pressure $p_{\rm Fe}$ of Fe atoms has to be equal to the vapour pressure of Fe atoms over solid iron, which is given by (law of mass-action[1])

$$\frac{1}{p_{\rm vap,Fe}(T)} = {\rm e}^{-\Delta G/RT}\,. \tag{10}$$

ΔG denotes here and in all of the following equations the Gibbs free enthalpy of formation of the substance under consideration (solid iron in the present case) from *free atoms*. From (9) and (10) we get

$$P = \frac{1+2\epsilon_{\rm He}}{2(1-f)\,\epsilon_{\rm Fe}}\,p_{\rm vap,Fe}(T)\,. \tag{11}$$

This uniquely defines, for any given temperature T, the total pressure P in a state where just the fraction f of the total available iron has condensed into solid iron. $f=0$ defines the limit curve in the P-T plane above and to the left of which no condensed iron can exist. We calculate the position of this limit curve using thermodynamic data for ΔG from Sharp & Huebner (1990). If not explicitly stated otherwise, in all of the following calculations thermodynamic data are taken from this source. Element abundances are that given by Anders & Grevesse (1989) with the updatings of Grevesse & Noels (1993). The result is shown in Fig. 3. Obviously, metallic iron is one of the most stable dust components in the disk which can be formed from the most abundant refractory elements.

The iron easely forms alloys with some other elements, especially with the somewhat less abundant Ni. Such solid solutions are not considered in this paper.

The limit curve for vapourisation of solid Mg is calculated in the same way as for iron and the result also is shown in Fig. 3. Obviously, no solid magnesium particles can exist in the disk.

4.2. Siliconoxide

Silicon forms the solid oxide SiO_2. This may be formed from the gas phase by for instance the reaction

$$\rm SiO \;+\; H_2O \;\longrightarrow\; SiO_2(s) \;+\; H_2\,.$$

The solid and the gas phase species are in chemical equilibrium if the partial pressures of the molecules satisfy

$$\frac{p_{\rm H_2}}{p_{\rm SiO}\,p_{\rm H_2O}} = {\rm e}^{-\Delta G/RT} = K_p(T) \tag{12}$$

[1] Recall that in a heterogeneous equilibrium the partial pressures of the solid components are set to unit pressure and do not explicitly show up in the expression. The solids do enter, however, into the equation via their Gibbs energy of formation

where $\Delta G = (\Delta G({\rm SiO_2}) + \Delta G({\rm H_2}) - \Delta G({\rm SiO}) - \Delta G({\rm H_2O}))$. Let f be the fraction of the totally available silicon bound into SiO_2. If no other condensed silicon compound is present, then the partial pressure of SiO molecules in the gas phase is $(1-f)\epsilon_{\rm Si}P_{\rm H}$ and if no oxygen is bound in any other one condensate, the partial pressure of H_2O in the gas phase is $(\epsilon_{\rm O}-\epsilon_{\rm C}-(1+f)\epsilon_{\rm Si})P_{\rm H}$. It follows

$$P = \frac{1+2\epsilon_{\rm He}}{4(1-f)\,\epsilon_{\rm Si}\,(\epsilon_{\rm O}-\epsilon_{\rm C}-(1+f)\epsilon_{\rm Si})\,K_p(T)}\,. \tag{13}$$

This, again, determines for any T the total pressure P of the gas phase in that state where just the fraction f of the silicon is condensed into SiO_2. The limit curve for stability of SiO_2 corresponds to $f=0$. This limit curve is shown in Fig. 3 for the temperature and pressure region of interest for protoplanetary accretion disks. Since the stability limit for SiO_2 is below and to the right of the stability limit of the Mg-Fe silicates (cf. Fig. 3) to be discussed later the SiO_2 is not expected to exist in a chemical equilibrium state.

The relation (13) does not depend on the special choice of a reaction considered for the formation of the SiO_2. Since we consider a thermodynamic equilibrium state, the principle of detailed balance holds according to which the equilibrium state does not depend on the special process responsible for its formation. Assuming any other reaction for the formation of SiO_2 would yield just the same limit curve. Thus we are free to choose in the present case, as well as in all of the following considerations, that reaction for the formation of a substance which is the most convenient one for calculational purposes.

The method used here and in the following considerations for calculating abundances of solid compounds is not as flexible as the method of minimization of the total Gibbs free energy of the system applied for calculating the abundances in a mixture of a big number of molecules, solid compounds, and solid solutions as implemented, for instance, in the codes used by Saxena & Eriksson (1986) or Sharp & Huebner (1990), but the approximate formulas to be developed in this paper are well suited for computational purposes if combined with semi analytic equations for the disk structure like that given in Sect. 6.1.

The molecule SiO alternatively can condense into the less stable solid siliconmonoxide. This may be of interest for circumstellar dust condensation (e.g. Gail & Sedlmayr 1998) but is of no interest for accretion disks.

4.3. Iron sulphide

One important component of the dust mixture seems to be solid FeS. We consider its formation by a reaction between solid Fe and H_2S molecules from the gas phase

$$\rm Fe(s) \;+\; H_2S \;\longrightarrow\; FeS(s) \;+\; H_2\,.$$

In chemical equilibrium the partial pressures of the molecules have to satisfy

$$\frac{p_{\rm H_2}}{p_{\rm H_2S}} = {\rm e}^{-\Delta G/RT} = K_p(T)\,, \tag{14}$$

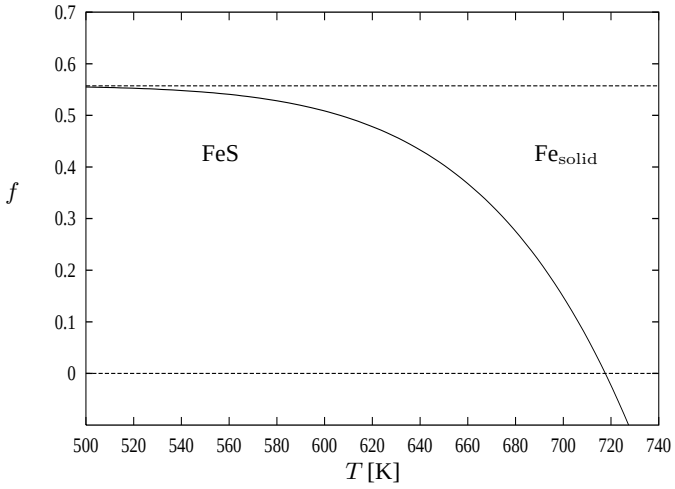

Fig. 4. Fraction f of metallic iron which is converted by H_2S into FeS (troilite) in matter with solar system element abundance.

where $\Delta G = \Delta G(\mathrm{FeS(s)}) + \Delta G(\mathrm{H_2}) - \Delta G(\mathrm{Fe(s)}) - \Delta G(\mathrm{H_2S})$. If we assume that the fraction f of the totally available iron has reacted to FeS then we have for the partial pressure of H_2S in the gas phase

$$p_{\mathrm{H_2S}} = \frac{2(\epsilon_{\mathrm{S}} - f\epsilon_{\mathrm{Fe}})}{1+2\epsilon_{\mathrm{He}}}\,P\,. \tag{15}$$

From (14) it follows for a chemical equilibrium state

$$\frac{P}{1+2\epsilon_{\mathrm{He}}}\,\frac{1+2\epsilon_{\mathrm{He}}}{2(\epsilon_{\mathrm{S}} - f\epsilon_{\mathrm{Fe}})\,P} = K_p(T)\,.$$

Here the pressure P of the gas phase drops from the expression. The solution for f of this equation

$$f = \frac{1}{\epsilon_{\mathrm{Fe}}}\left(\epsilon_{\mathrm{S}} - \frac{1}{2K_p(T)}\right) \tag{16}$$

only depends on the temperature. The maximum fraction of the iron which can be converted into FeS equals the abundance ratio $\epsilon_{\mathrm{S}}/\epsilon_{\mathrm{Fe}} = 0.56$. If the quantity f calculated from Eq. (16) for a certain temperature T takes a value in the interval $0 \le f \le 0.56$, then for this temperature the iron metal is partially converted into solid FeS. If there results a value of $f < 0$, then all the iron is present as the free metal and we have to put $f = 0$ in this case. Fig. 4 shows the result for f for solar system element abundances. An inspection of the figure shows that the conversion of FeS to Fe is extended over a broad temperature region. The reduction of FeS starts to become significant at 500 K, gradually increases with increasing T and is completed at a temperature of $T \approx 720$ K. Above this temperature, the iron would be present as the free metal and no FeS can exist at such temperatures due to reduction of FeS by the abundant hydrogen. Below this temperature the iron would form FeS due to sulphidisation by H_2S, but this cannot convert all of the iron into FeS since S is less abundant than Fe. If iron is not bound in some other solid, the excess over S would be converted below 370 K into iron oxide. The kinetics of the formation of FeS has been studied in detail by Lauretta et al. (1996).

4.4. Iron oxides and hydrides

Iron and magnesium may form oxides and hydroxides. Such compounds occur only at temperatures well below 400 K (e.g. Fegley 1989) and are of no interest for the warm inner parts of an accretion disk where the main dust materials are destroyed. The iron oxides and hydroxides will be considered in a separate paper on iron grains in accretion disks (Finocchi & Gail 1998).

4.5. Equilibrium chemistry of the Mg-Fe ortho-silicates

The dust model of Pollak et al. (1994) considers two types of magnesium-iron silicates:

- The ortho silicates with the composition $\mathrm{Mg_{2x}Fe_{2(1-x)}SiO_4}$. They form a continuous series of compounds with $0 \le x \le 1$. The two members at the endpoints of this series are fayalite ($x = 0$) and forsterite ($x = 1$). The intermediate case is known as olivine. In the P94 model $x = 0.7$ is assumed.
- The meta-silicates with the composition $\mathrm{Mg}_x\mathrm{Fe}_{1-x}\mathrm{SiO_3}$. They form a continuous series of compounds with $0 \le x \le 1$. The two members at the endpoints of this series are ferrosilite ($x = 0$) and enstatite ($x = 1$). The intermediate case is known as orthopyroxene. In the P94 model $x = 0.7$ is assumed.

First we consider the ortho-silicates. We determine the limit curves for the stability of the extreme members of this series. The law of mass action for the reaction of formation of forsterite ($\mathrm{Mg_2SiO_4}$) from gas phase species according to the reaction

$$2\mathrm{Mg} + \mathrm{SiO} + 3\mathrm{H_2O} \longrightarrow \mathrm{Mg_2SiO_4(s)} + 3\mathrm{H_2}$$

is

$$\frac{p_{\mathrm{H_2}}^3}{p_{\mathrm{Mg}}^2\,p_{\mathrm{SiO}}\,p_{\mathrm{H_2O}}^3} = \mathrm{e}^{-\Delta G/RT} = K_p(T) \tag{17}$$

where $\Delta G = \Delta G(\mathrm{Mg_2SiO_4(s)}) + 3\Delta G(\mathrm{H_2}) - 2\Delta G(\mathrm{Mg}) - \Delta G(\mathrm{SiO}) - 3\Delta G(\mathrm{H_2O})$. Let f be the fraction of the silicon bound in $\mathrm{Mg_2SiO_4}$. If there exists no other dust condensate than this one, the partial pressure of SiO in the gas phase is $(1-f)\epsilon_{\mathrm{Si}}P_{\mathrm{H}}$, that of Mg is $(\epsilon_{\mathrm{Mg}} - 2f\epsilon_{\mathrm{Si}})P_{\mathrm{H}}$ and that of water vapour is $(\epsilon_{\mathrm{O}} - \epsilon_{\mathrm{C}} - (1+3f)\epsilon_{\mathrm{Si}})P_{\mathrm{H}}$. Inserting this into (17) yields

$$P^3 = \frac{(1+2\epsilon_{\mathrm{He}})^3\,K_p^{-1}(T)}{2^6(1-f)\,\epsilon_{\mathrm{Si}}\,(\epsilon_{\mathrm{Mg}} - 2f\epsilon_{\mathrm{Si}})^2\,(\epsilon_{\mathrm{O}} - \epsilon_{\mathrm{C}} - (1+3f)\epsilon_{\mathrm{Si}})^3}\,. \tag{18}$$

The limit curve $f = 0$ for complete destruction of $\mathrm{Mg_2SiO_4}$ is shown in Fig. 3. If Mg is replaced by Fe in this equation, one obtains the corresponding equation for fayalite ($\mathrm{Fe_2SiO_4}$). The limit curve $f = 0$ for complete destruction of $\mathrm{Fe_2SiO_4}$ by volatilisation into gaseous components is shown in Fig. 3, too. We observe that forsterite is much more stable than fayalite.

Next we consider the magnesium-iron silicates (olivines) with a mixed composition $\mathrm{Mg_{2x}Fe_{2(1-x)}SiO_4}$ with $x \in [0,1]$.

We assume that the members of this series form a solid solution of forsterite and fayalite. The free enthalpy of formation of one mole of the mixture from x moles of forsterite and $1-x$ moles of fayalite is given by the weighted mean of the free enthalpy of formation of both components and the mixing entropy term

$$\Delta G(\mathrm{Mg}_{2x}\mathrm{Fe}_{2(1-x)}\mathrm{SiO_4}) = x\Delta G(\mathrm{Mg_2SiO_4}) + (1-x)\Delta G(\mathrm{Fe_2SiO_4}) + 2RT\left[x\ln x + (1-x)\ln(1-x)\right] \quad (19)$$

(Atkins 1994). We consider the conversion of forsterite into olivine by means of the reaction

$$\mathrm{Mg_2SiO_4(s)} \;+\; 2(1-x)\mathrm{Fe} \;\longrightarrow\; \mathrm{Mg}_{2x}\mathrm{Fe}_{2(1-x)}\mathrm{SiO_4(s)} \;+\; 2(1-x)\mathrm{Mg}\,.$$

In a chemical equilibrium state between the gas phase and olivine, the partial pressures of Mg and Fe atoms in the gas phase satisfy the law of mass action

$$\frac{p_{\mathrm{Mg}}^{2(1-x)}}{p_{\mathrm{Fe}}^{2(1-x)}} = \mathrm{e}^{-\Delta G_x/RT} \quad (20)$$

where $\Delta G_x = \Delta G(\mathrm{Mg}_{2x}\mathrm{Fe}_{2(1-x)}\mathrm{SiO_4(s)}) - \Delta G(\mathrm{Mg_2SiO_4(s)}) + 2(1-x)\left(\Delta G(\mathrm{Mg}) - \Delta G(\mathrm{Fe})\right)$ is the change of free enthalpy in the conversion of forsterite into olivine. It follows

$$\frac{p_{\mathrm{Mg}}}{p_{\mathrm{Fe}}} = \exp\Big[-\frac{\Delta G_x}{2(1-x)RT}\Big] = K_x(T)\,, \quad (21)$$

where we denote the equilibrium constant for the conversion by K_x. This equation determines the pressure ratio of Mg and Fe atoms in a chemical equilibrium state with olivine. For the equilibrium constant K_x we have

$$K_x(T,x) = \exp\Big[-\frac{\Delta G(\mathrm{fay.}) - \Delta G(\mathrm{for.})}{2RT} - \frac{\Delta G_{\mathrm{mix}}}{2(1-x)RT}\Big] \quad (22)$$

where

$$\Delta G_{\mathrm{mix}} = 2RT\left[x\ln x + (1-x)\ln(1-x)\right]\,. \quad (23)$$

The temperature dependence of K_x for some values of x is shown in Fig. 5.

If f is the fraction of silicon bound in the olivine, the partial pressures of Mg and Fe in the gas phase are $(\epsilon_{\mathrm{Mg}} - 2xf\epsilon_{\mathrm{Si}})P_{\mathrm{H}}$ and $(\epsilon_{\mathrm{Fe}} - 2(1-x)f\epsilon_{\mathrm{Si}})P_{\mathrm{H}}$, respectively. Then

$$\frac{\epsilon_{\mathrm{Mg}} - 2xf\epsilon_{\mathrm{Si}}}{\epsilon_{\mathrm{Fe}} - 2(1-x)f\epsilon_{\mathrm{Si}}} = K_x(T,x)\,. \quad (24)$$

The degree of condensation f is determined by Eq. (18) where the term $\epsilon_{\mathrm{Mg}} - 2f\epsilon_{\mathrm{Si}}$ has to be replaced by $\epsilon_{\mathrm{Mg}} - 2xf\epsilon_{\mathrm{Si}}$. Both Eqs. (24) and (18), together determine the amount and composition of a magnesium-iron silicate condensed in a chemical equilibrium state. We can solve (24) for f

$$f = \frac{\epsilon_{\mathrm{Mg}} - \epsilon_{\mathrm{Fe}}K_x}{2\epsilon_{\mathrm{Si}}(x - K_x(1-x))}\,. \quad (25)$$

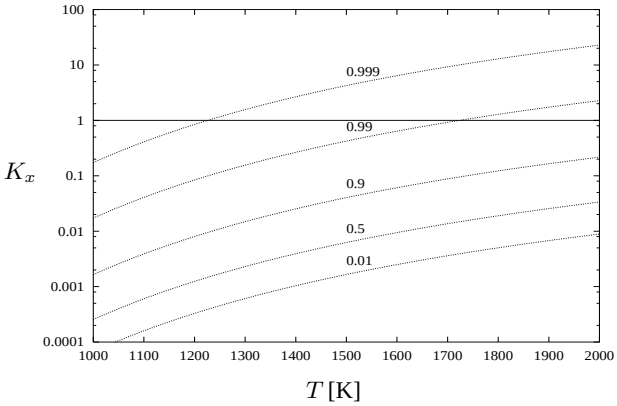

Fig. 5. Equilibrium constant $K_x(T)$ for the conversion of forsterite into olivine. The values of x are indicated at the curves

For instance, if $x = .5$ then inspection of Fig. 5 shows $K_x \ll 1$ and then $f \approx 1$, as is to be expected from solar system element abundances. Complete destruction of the silicate means $f = 0$ which means according to (25) $K_x = \epsilon_{\mathrm{Mg}}/\epsilon_{\mathrm{Fe}} = 1.29$ (element abundances according to Anders & Grevesse (1989)). An inspection of Fig. 5 shows that in this case $(1-x) \ll 1$. At the stability limit the material has nearly the composition of pure forsterite. The reason for this is simple: at sufficiently high temperature the fayalite component is distilled off from the solution.

For given x and T Eq. (25) determines f and then from Eq. (18) we can determine the total gas pressure corresponding to this state. Equilibrium curves in the P-T plane for some interesting values of x are shown in Fig. 6. An inspection of the figure shows that in a broad temperature region below the limit for decomposition of the olivine the chemical equilibrium composition of olivine would be that of nearly pure forsterite. Only at temperatures at least 200 K below the stability limit would substantial amounts of Fe be incorporated into the silicate. Inspection of Fig. 3 or Fig. 6 shows that the iron condenses as the free iron metal at similar temperatures as the olivine and hence in a broad region the chemical equilibrium composition of the condensate corresponds to a mixture of nearly pure forsterite and metallic iron particles!

In constructing Fig. 6 we have assumed that iron is not condensed. The formation of solid iron would reduce the pressure of Fe atoms in the gas phase and this would favour a value of x even closer to unity.

4.6. The Mg-Fe meta-silicates

The same type of consideration yields for the curve of constant degree f of condensation of silicon into the meta-silicate enstatite

$$P = \frac{(1+2\epsilon_{\mathrm{He}})\,K_p^{-\frac{1}{2}}(T)}{4(1-f)^{\frac{1}{2}}\,\epsilon_{\mathrm{Si}}^{\frac{1}{2}}\,(\epsilon_{\mathrm{Mg}} - f\epsilon_{\mathrm{Si}})^{\frac{1}{2}}\,(\epsilon_{\mathrm{O}} - \epsilon_{\mathrm{C}} - (1+2f)\epsilon_{\mathrm{Si}})} \quad (26)$$

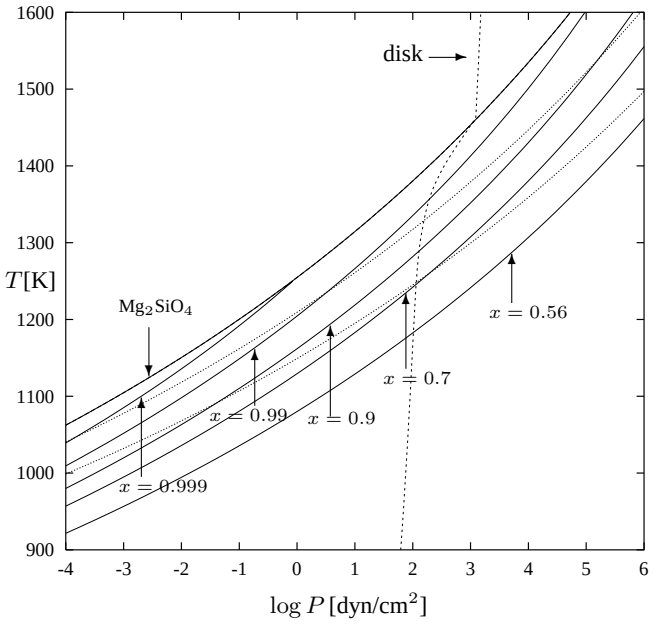

Fig. 6. Limit curves for conversion of forsterite into olivine. The numbers denote the value of the stoichiometric coefficient x for olivine with composition $Mg_{2x}Fe_{2(1-x)}SiO_4$. The uppermost full line is the stability limit of pure forsterite ($x = 1$). The upper dotted line shows the stability limit of enstatite, the lower one where 90% of the forsterite is converted into enstatite. The dashed line shows the P-T stratification in the central plane of a protoplanetary disk model for comparison.

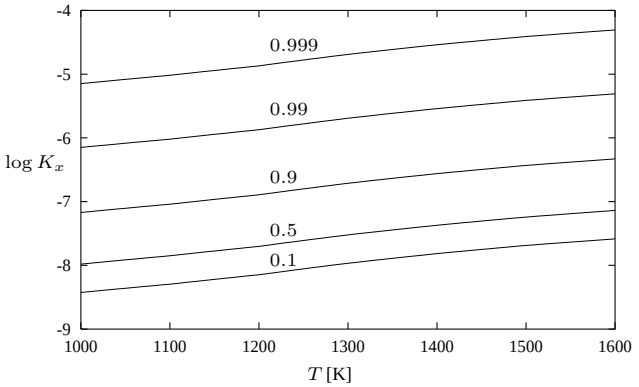

Fig. 7. Equilibrium constant $K_x(T)$ for the conversion of enstatite into orthopyroxene. The values of x are indicated at the curves

and the corresponding equation for ferrosilite with Mg replaced by Fe. The limit curve $f = 0$ for complete destruction of $MgSiO_3$ is shown in Fig. 3. It is nearly as stable as Mg_2SiO_4 and is destroyed at an only slightly lower temperature than forsterite. This means, that there exists the possibility that ortho- and meta-silicates may coexist in a chemical equilibrium state. We shall come back to this point below and consider first the conversion of enstatite into orthopyroxene.

We consider the magnesium-iron silicates with a mixed composition $Mg_xFe_{(1-x)}SiO_3$ with $x \in [0, 1]$. They are assumed to form an ideal solid solution of ferrosilite ($x = 0$) and enstatite ($x = 1$). The free enthalpy of formation of one mole of the mixture from x moles of enstatite and $1 - x$ moles of ferrosilite is given by

$$\Delta G(\mathrm{Mg_xFe_{(1-x)}SiO_3(s)}) = x\Delta G(\mathrm{MgSiO_3(s)}) + (1-x)\Delta G(\mathrm{FeSiO_3(s)}) + RT\left[x\ln x + (1-x)\ln(1-x)\right]. \quad (27)$$

Now, we consider the conversion of enstatite into orthopyroxene by means of the reaction

$$\mathrm{MgSiO_3(s)} + (1-x)\mathrm{Fe} \rightarrow \mathrm{Mg_xFe_{(1-x)}SiO_3(s)} + (1-x)\mathrm{Mg}\,.$$

In chemical equilibrium the partial pressures of Mg and Fe atoms in the gas phase satisfy

$$\frac{p_{\mathrm{Mg}}^{(1-x)}}{p_{\mathrm{Fe}}^{(1-x)}} = \mathrm{e}^{-\Delta G_x/RT} \quad (28)$$

where $\Delta G_x = \Delta G(\mathrm{Mg_xFe_{(1-x)}SiO_3}) - \Delta G(\mathrm{MgSiO_3}) + (1-x)\left(\Delta G(\mathrm{Mg}) - \Delta G(\mathrm{Fe})\right)$ is the change of free enthalpy in the conversion of enstatite into orthopyroxene. It follows

$$\frac{p_{\mathrm{Mg}}}{p_{\mathrm{Fe}}} = \exp\Big[-\frac{\Delta G_x}{(1-x)RT}\Big] = K_x(T)\,, \quad (29)$$

where again we denote the equilibrium constant for the conversion by K_x. For the equilibrium constant K_x we obtain

$$K_x(T,x) = \exp\Big[-\frac{\Delta G(\mathrm{fer.}) - \Delta G(\mathrm{enst.})}{RT} - \frac{\Delta G_{\mathrm{mix}}}{(1-x)RT}\Big] \quad (30)$$

where

$$\Delta G_{\mathrm{mix}} = RT\left[x\ln x + (1-x)\ln(1-x)\right]. \quad (31)$$

The result for K_x for some values of x are shown in Fig. 7. Data for $FeSiO_3$ are taken from Saxena & Eriksson (1986). K_x is very small since the conversion of $MgSiO_3$ into $FeSiO_3$ is strongly endothermic with $\Delta H = +171$ kcal/ Mol.

If f denotes the fraction of silicon bound in orthopyroxene, the partial pressures of Mg and Fe in the gas phase are $(\epsilon_{\mathrm{Mg}} - xf\epsilon_{\mathrm{Si}})P_{\mathrm{H}}$ and $(\epsilon_{\mathrm{Fe}} - (1-x)f\epsilon_{\mathrm{Si}})P_{\mathrm{H}}$, respectively. Then

$$\frac{\epsilon_{\mathrm{Mg}} - xf\epsilon_{\mathrm{Si}}}{\epsilon_{\mathrm{Fe}} - (1-x)f\epsilon_{\mathrm{Si}}} = K_x(T,x)\,. \quad (32)$$

Since K_x for the relevant temperatures is of the order of 10^{-5} this requires $xf = \epsilon_{\mathrm{Mg}}/\epsilon_{\mathrm{Si}}$. Since x and f by definition both are less than unity and $\epsilon_{\mathrm{Mg}} > \epsilon_{\mathrm{Si}}$ for a solar system like element composition there exists no solution of (32) for x if only the meta-silicate would exist. In this case only pure enstatite exists in chemical equilibrium. If part of the Mg is bound in ortho-silicates, the orthopyroxenes with $x < 1$ may exist.

Next we consider the possibility of a coexistence of ortho- and meta-silicates. Since the iron content of the silicates in any case is small, as we have seen, we can restrict our considerations to pure Mg-silicates. As can be seen from Fig. 3 the ortho-silicate is stable up to a slightly higher temperature than the

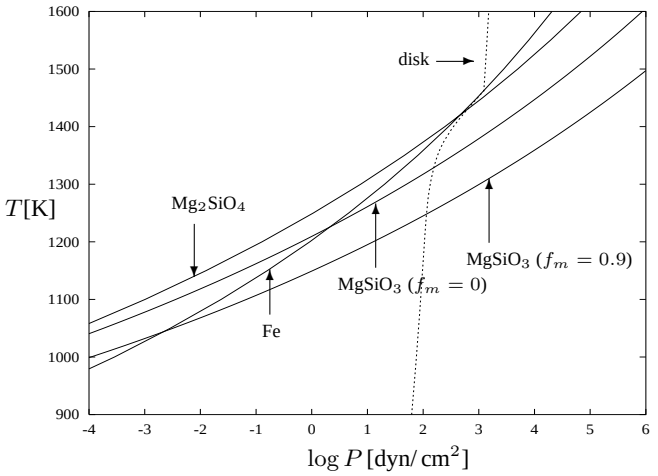

Fig. 8. Equilibrium between forsterite (Mg_2SiO_4) and enstatite ($MgSiO_3$) and the limit curves for stability of forsterite and solid iron. The dashed line shows the P-T stratification in the central plane of a protoplanetary disk model.

meta-silicate. In a chemical equilibrium state with the hydrogen rich gas phase, coexistence between ortho- and meta-silicates means

$$\mathrm{Mg_2SiO_4(s)} \,+\, \mathrm{H_2} \,\longleftrightarrow\, \mathrm{MgSiO_3(s)} \,+\, \mathrm{Mg} \,+\, \mathrm{H_2O}\,. \quad (33)$$

According to the law of mass-action the partial pressures of the gaseous species have to satisfy in equilibrium

$$\frac{p_{\mathrm{Mg}}p_{\mathrm{H_2O}}}{p_{\mathrm{H_2}}} = \mathrm{e}^{-\Delta G/RT} = K_c(T) \quad (34)$$

where $\Delta G = \Delta G(\mathrm{MgSiO_3(s)}) + \Delta G(\mathrm{Mg}) + \Delta G(\mathrm{H_2O}) - \Delta G(\mathrm{Mg_2SiO_4(s)}) - \Delta G(\mathrm{H_2})$. Assuming that no other dust species are present than the two species presently under consideration the partial pressure of Mg in the gas phase is $(\epsilon_{\mathrm{Mg}} - (2f_o + f_m)\epsilon_{\mathrm{Si}})P_{\mathrm{H}}$, the partial pressure of H_2O is $(\epsilon_{\mathrm{O}} - \epsilon_{\mathrm{C}} - (3f_o + 2f_m + 1)\epsilon_{\mathrm{Si}})P_{\mathrm{H}}$, and the partial pressure of H_2 is $\frac{1}{2}P_{\mathrm{H}}$. f_o and f_m denote the fraction of the silicon condensed in the ortho- and meta-silicate, respectively. It follows

$$P = \frac{(1 + 2\epsilon_{\mathrm{He}})K_c(T)}{4(\epsilon_{\mathrm{Mg}} - (2f_o + f_m)\epsilon_{\mathrm{Si}})\,(\epsilon_{\mathrm{O}} - \epsilon_{\mathrm{C}} - (3f_o + 2f_m + 1)\epsilon_{\mathrm{Si}})}\,. \quad (35)$$

This is the total pressure P of the gas phase in a chemical equilibrium state between the ortho- and meta-silicate for given f_o, f_m, and T. The limit where enstatite just starts to be converted into enstatite is defined by $f_m = 0$. Additionally we have Eq. (18) for the equilibrium between forsterite and the gas phase. Adapted to the present case it reads as follows

$$P = \frac{1 + 2\epsilon_{\mathrm{He}}}{4}\,\left[\frac{1}{K_p(T)(1 - f_o - f_m)\epsilon_{\mathrm{Si}}}\right]^{\frac{1}{3}} \cdot \frac{1}{(\epsilon_{\mathrm{Mg}} - (2f_o + f_m)\epsilon_{\mathrm{Si}})^{\frac{2}{3}}\,(\epsilon_{\mathrm{O}} - \epsilon_{\mathrm{C}} - (3f_o + 2f_m + 1)\epsilon_{\mathrm{Si}})}\,. \quad (36)$$

Equating this to (35) yields the equation

$$K_c^3\,K_p = \frac{\epsilon_{\mathrm{Mg}} - (2f_o + f_m)\epsilon_{\mathrm{Si}}}{(1 - f_o - f_m)\epsilon_{\mathrm{Si}}} \quad (37)$$

for f_o in terms of f_m or vice versa. This relation only depends on the temperature T but not on the pressure P.

Let $f_m = z f_o$ and solve for f_o:

$$f_o = \frac{\epsilon_{\mathrm{Mg}} - \epsilon_{\mathrm{Si}}K_c^3K_p}{(2 + z - (1 + z)\,K_c^3K_p)\epsilon_{\mathrm{Si}}}\,. \quad (38)$$

Using this in (36) one obtains for given T the total pressure P in an equilibrium state where the abundance of enstatite is a given multiple z of the abundance of forsterite. At the stability limit of enstatite we have $z = 0$. This defines a limit curve in the P-T plane, above and to the left of which only forsterite exists in a chemical equilibrium state and below and to the right of which forsterite and enstatite both coexist. Fig. 8 shows this limit curve for the pressure and temperature conditions of interest for the protoplanetary accretion disk. The figure also shows the curve with $z = 9$ where most (90%) of the condensed silicate in chemical equilibrium forms enstatite. Thus, only in a rather narrow strip of the P-T plane the forsterite forms a significant fraction of the mixture of silicates. At low temperatures the enstatite dominates in chemical equilibrium and the abundance of the forsterite component decreases gradually with decreasing temperature. It does not drop, however, below an abundance of $f \approx 0.08$.

4.7. Iron-magnesium-silicon compounds in the disk

According to our above findings the following compounds of Si, Fe, and Mg are formed in chemical equilibrium:

1. Olivine and Orthopyroxene. At low temperatures the magnesium is consumed by the formation of olivine and orthopyroxene. The orthopyroxene is the more abundant of the two magnesium silicates up to temperatures close below the stability limit for the conversion of orthopyroxene into olivine. Above this stability limit the magnesium forms olivine up to the stability limit of this compound. The iron content of olivine and orthopyroxene is small, especially at elevated temperatures. Hence olivine in an environment with Solar System abundances in fact is nearly pure forsterite and orthopyroxene is nearly pure enstatite.
2. Iron. The orthopyroxene and olivine consume only a small fraction of the available Fe. The excess of the iron is condensed into pure iron particles. The stability limit of condensed iron crosses the stability limit of forsterite. At low pressures condensed forsterite exists up to slightly higher temperatures than iron while for high pressures iron exists up to slightly higher temperatures then olivine.
3. Troilite. At low temperatures the iron forms with the available S solid FeS (troilite). Since the Fe element abundance exceeds the S abundance, the excess of Fe over S forms pure iron particles.

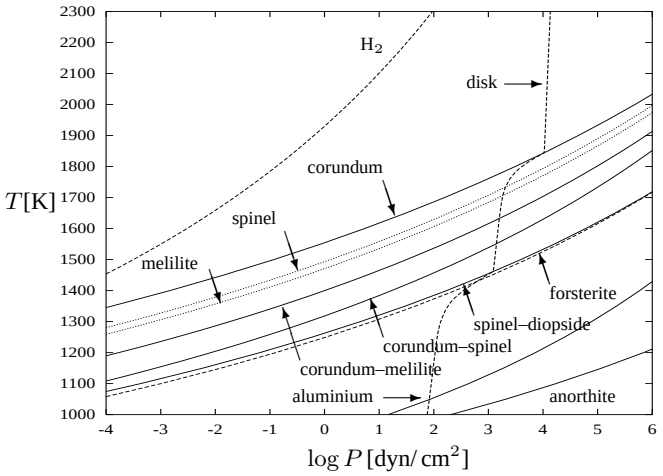

Fig. 9. Stability limits of solid aluminium and aluminium-calcium compounds against volatilisation and stability limits for conversion of some aluminium and aluminium-calcium compounds. The dashed lines show the dissociation limits of H_2, the pressure-temperature stratification in the midplane of the accretion disk model, and the stability limit of the most refractory of the silicates, the forsterite (Mg_2SiO_4).

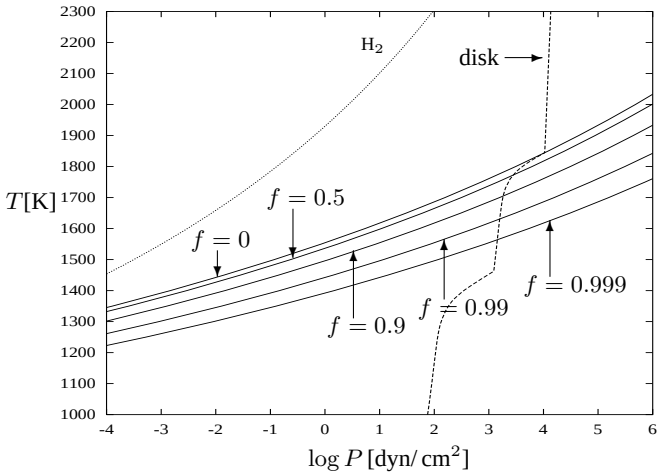

Fig. 10. Equilibrium condensation of corundum (Al_2O_3). The numbers denote the fraction f of the aluminium condensed into Al_2O_3. The dotted line shows the dissociation limit of H_2 and the dashed line the pressure-temperature stratification in the midplane of the accretion disk model. The upper and lower inflections in this line correspond to the stability limits of corundum and olivine, respectively.

As our discussion of the equilibrium abundances of Si,Fe, and Mg compounds shows, these compounds occur in any environment in the above order of temperature. Only the precise value of the temperatures where the different compounds appear or disappear depend on the details of the P-T stratification in the accretion disk.

5. Equilibrium chemistry of the Al-Ca complex

Aluminium and aluminium-calcium compounds tend to be more stable than magnesium-iron silicates. For this reason there exists a certain zone in the inner part of the accretion disk where no silicate dust exists but the refractory aluminium compounds do exist and dominate the extinction of the disk material and, by this, the disk structure. From the results of the calculations of Grossman (1972), Saxena & Eriksson (1986), and Sharp & Huebner (1990) for the equilibrium composition of an oxygen rich mixture we can see, that five different abundant aluminium and calcium compounds can be formed from a solar system element mixture which may be important for the disk structure: (i) aluminium oxide or corundum (Al_2O_3), (ii) melilite, a solid solution of gehlenite ($Al_2Ca_2SiO_7$) and åkermanite ($MgSiCa_2SiO_7$), (iii) spinel ($MgAl_2O_4$), (iv) diopside ($CaMgSi_2O_6$), and (v) anorthite ($CaAl_2Si_2O_8$).

5.1. Aluminium oxide

The most refractory of these compounds is the solid aluminium oxide due to its extremely high energy of formation. Molecules formed from Al and O, on the other hand, do not have a particular high bond energy. At such temperatures where the Al_2O_3 disappears, the particle densities of the aluminium bearing molecules AlO and AlO_2 in the gas phase are small compared to the particle density of the free Al atoms. The oxygen at the same temperature is bound mainly in H_2O, CO, and SiO. Since CO and SiO are not involved in the chemistry of Al_2O_3 formation or destruction, we assume that the Al_2O_3 is formed by the reaction

$$2\mathrm{Al} \;+\; 3\mathrm{H_2O} \;\longrightarrow\; \mathrm{Al_2O_3(s)} \;+\; 3\mathrm{H_2}$$

from gas phase species. In a state of thermodynamic equilibrium between the molecules involved in this reaction and the solid, the partial pressures of the gas phase species satisfy the law of mass action

$$\frac{p_{\mathrm{H_2}}^3}{p_{\mathrm{Al}}^2\, p_{\mathrm{H_2O}}^3} = \mathrm{e}^{-\Delta G/RT} = K_p(T) \tag{39}$$

where $\Delta G = \Delta G(\mathrm{Al_2O_3(s)}) + 3\Delta G(\mathrm{H_2}) - 3\Delta G(\mathrm{H_2O})$. Assuming that the fraction f of the aluminium is condensed into corundum the partial pressure of free Al atoms in the gas phase is $p_{\mathrm{Al}} = (1-f)\,\epsilon_{\mathrm{Al}}\,P_{\mathrm{H}}$ and if no other oxygen bearing condensate than the Al_2O_3 is present the partial pressure of H_2O in the gas phase is $p_{\mathrm{H_2O}} = (\epsilon_{\mathrm{O}} - \epsilon_{\mathrm{C}} - \epsilon_{\mathrm{Si}} - \frac{3}{2} f \epsilon_{\mathrm{Al}})\,P_{\mathrm{H}}$. From (39) we obtain

$$P^2 = \frac{(1+2\epsilon_{\mathrm{He}})^2}{2^5\,(1-f)^2\,\epsilon_{\mathrm{Al}}^2\,(\epsilon_{\mathrm{O}} - \epsilon_{\mathrm{C}} - \epsilon_{\mathrm{Si}} - \frac{3}{2} f \epsilon_{\mathrm{Al}})^3\,K_p(T)}\,. \tag{40}$$

Fig. 10 shows the resulting curves for some values of f for pressure and temperature conditions of interest for protoplanetary accretion disks. $f = 0$ corresponds to the limit curve left and above of which no condensed Al_2O_3 exists. A comparison with Fig. 3 or Fig. 9 shows that the Al_2O_3 indeed is stable up to a much higher temperature than forsterite, the most refractory of the silicates. There exist a region $\approx 300\,\mathrm{K}$ wide in temperature where corundum is stable but not any one of the silicates.

5.2. Melilite

The most stable Al-Ca and Ca-Mg silicates at high temperature are gehlenite ($Ca_2Al_2SiO_7$) and åkermanite, ($Ca_2MgSi_2O_7$) which form a solid solution called melilite. Since the åkermanite has only a small concentration in the mixture (Saxena & Eriksson 1983) we neglect in our calculation this component of melilite.

Consider the hypothetical case that no other aluminium bearing condensate then gehlenite is present. At the relevant temperatures the gas phase species available to form gehlenite are free Ca and Al atoms, and SiO and H_2O molecules. The gehlenite then may be formed by the reaction

$$2\mathrm{Ca} + 2\mathrm{Al} + \mathrm{SiO} + 6\mathrm{H_2O} \longrightarrow \mathrm{Ca_2Al_2SiO_7(s)} + 6\mathrm{H_2}\,. \quad (41)$$

According to the law of mass action the partial pressures of the molecular species in the gas phase have to satisfy

$$\frac{p_{\mathrm{H_2}}^6}{p_{\mathrm{Ca}}^2\, p_{\mathrm{Al}}^2\, p_{\mathrm{SiO}}\, p_{\mathrm{H_2O}}^6} = \mathrm{e}^{-\Delta G/RT} = K_p(T) \quad (42)$$

where $\Delta G = \Delta G(\mathrm{geh}) + 6\Delta G(\mathrm{H_2}) - \Delta G(\mathrm{SiO}) - 2\Delta G(\mathrm{Ca}) - 2\Delta G(\mathrm{Al}) - 6\Delta G(\mathrm{H_2O})$. If a fraction g of the calcium is bound in gehlenite, we have for the partial pressures of the free atoms $p_{\mathrm{Ca}} = (1-g)\,\epsilon_{\mathrm{Ca}}\,P_{\mathrm{H}}$, $p_{\mathrm{Al}} = (\epsilon_{\mathrm{Al}} - g\epsilon_{\mathrm{Ca}})\,P_{\mathrm{H}}$, and for the molecules $p_{\mathrm{SiO}} = (\epsilon_{\mathrm{Si}} - \frac{1}{2}g\epsilon_{\mathrm{Ca}})\,P_{\mathrm{H}}$, $p_{\mathrm{H_2O}} = (\epsilon_{\mathrm{O}} - \epsilon_{\mathrm{C}} - \epsilon_{\mathrm{Si}} - \frac{7}{2}g\epsilon_{\mathrm{Ca}})\,P_{\mathrm{H}}$. It follows

$$P^5 = \frac{(1+2\epsilon_{\mathrm{He}})^5}{2^{11}\,(1-g)^2\epsilon_{\mathrm{Ca}}^2(\epsilon_{\mathrm{Al}} - g\epsilon_{\mathrm{Ca}})^2(\epsilon_{\mathrm{Si}} - \frac{1}{2}g\epsilon_{\mathrm{Ca}})} \cdot \frac{1}{(\epsilon_{\mathrm{O}} - \epsilon_{\mathrm{C}} - \epsilon_{\mathrm{Si}} - \frac{7}{2}g\epsilon_{\mathrm{Ca}})^6 K_p(T)}\,.$$

The curve with $g = 0$ corresponds to the stability limit of gehlenite. As can be seen from Fig. 9 at the upper stability limit for volatilisation of gehlenite the corundum is stable. The aluminium liberated by the volatilisation of gehlenite then forms solid corundum. Thus, gehlenite does not disappear by decomposition into gaseous species as in reaction (41) but it is converted into corundum instead.

The relevant reaction for formation of gehlenite from corundum (or vice versa) is

$$\mathrm{Al_2O_3(s)} + 2\mathrm{Ca} + \mathrm{SiO} + 3\mathrm{H_2O} \longrightarrow \mathrm{Ca_2Al_2SiO_7(s)} + 3\mathrm{H_2}\,.$$

The partial pressures of the gaseous species in a chemical equilibrium state between gehlenite and corundum have to satisfy

$$\frac{p_{\mathrm{H_2}}^3}{p_{\mathrm{Ca}}^2\, p_{\mathrm{SiO}}\, p_{\mathrm{H_2O}}^3} = \mathrm{e}^{-\Delta G/RT} = K_p(T) \quad (43)$$

where $\Delta G = \Delta G(\mathrm{geh}) + 3\Delta G(\mathrm{H_2}) - \Delta G(\mathrm{cor}) - \Delta G(\mathrm{SiO}) - 3\Delta G(\mathrm{H_2O})$. If the fraction g of the calcium is condensed into gehlenite and the fraction f of the aluminium into corundum, we have for the partial pressures of the gas phase species $p_{\mathrm{Al}} = ((1-f)\epsilon_{\mathrm{Al}} - g\epsilon_{\mathrm{Ca}})\;P_{\mathrm{H}}$ and $p_{\mathrm{H_2O}} = (\epsilon_{\mathrm{O}} - \epsilon_{\mathrm{C}} - \epsilon_{\mathrm{Si}} - \frac{3}{2}f\epsilon_{\mathrm{Al}} - \frac{7}{2}g\epsilon_{\mathrm{Ca}})\,P_{\mathrm{H}}$. The partial pressures of SiO and Ca are the same as in the previous case. We obtain from (43)

$$P^3 = \frac{(1+2\epsilon_{\mathrm{He}})^3}{2^6(1-g)^2\epsilon_{\mathrm{Ca}}^2(\epsilon_{\mathrm{Si}} - \frac{1}{2}g\epsilon_{\mathrm{Ca}})} \cdot \frac{1}{(\epsilon_{\mathrm{O}} - \epsilon_{\mathrm{C}} - \epsilon_{\mathrm{Si}} - \frac{3}{2}f\epsilon_{\mathrm{Al}} - \frac{7}{2}g\epsilon_{\mathrm{Ca}})^3\,K_p(T)} \quad (44)$$

The resulting curves in the P-T plane for some values of g are shown in Fig. 11. $g = 0$ again determines the upper limit curve for stability of melilite. This stability limit is also shown in Fig. 9. There exists a strip in the P-T plane with $\approx 150\,\mathrm{K}$ width in temperature in which corundum is the most stable aluminium compound. Below this at lower temperatures part of the corundum is converted into gehlenite.

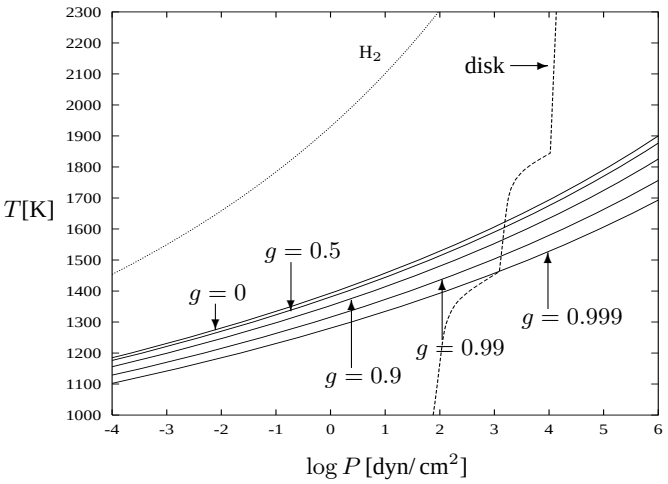

Fig. 11. Equilibrium condensation of gehlenite ($Ca_2Al_2SiO_7$). The numbers denote the fraction g of the calcium condensed into gehlenite. The dotted line shows the dissociation limit of H_2 and the dashed line the pressure-temperature stratification in the midplane of the accretion disk model. The upper and lower inflections in this line correspond to the stability limits of corundum and olivine, respectively.

The fraction f of aluminium condensed into corundum in the presence of gehlenite is given by (40) which now reads as

$$P^2 = \frac{(1+2\epsilon_{\mathrm{He}})^2}{2^5\;(\epsilon_{\mathrm{Al}} - f\epsilon_{\mathrm{Al}} - g\epsilon_{\mathrm{Ca}})^2} \cdot \frac{1}{(\epsilon_{\mathrm{O}} - \epsilon_{\mathrm{C}} - \epsilon_{\mathrm{Si}} - \frac{3}{2}f\epsilon_{\mathrm{Al}} - \frac{7}{2}g\epsilon_{\mathrm{Ca}})^3\,K_c(T)}\,,$$

where $K_c(T)$ denotes the equilibrium constant of corundum. Neglecting the small fraction of the oxygen bound in melilite and corundum and combining the two equations for P we obtain

$$f = 1 - g\frac{\epsilon_{\mathrm{Ca}}}{\epsilon_{\mathrm{Al}}} - \frac{(1-g)^{\frac{2}{3}}\,\epsilon_{\mathrm{Ca}}^{\frac{2}{3}}\,(\epsilon_{\mathrm{Si}} - \frac{1}{2}g\epsilon_{\mathrm{Ca}})^{\frac{1}{3}}\,K_p^{\frac{1}{3}}}{\epsilon_{\mathrm{Al}}\,2^{\frac{1}{2}}\,(\epsilon_{\mathrm{O}} - \epsilon_{\mathrm{C}} - \epsilon_{\mathrm{Si}})^{\frac{1}{2}}\,K_c^{\frac{1}{2}}} \quad (45)$$

Eqs. (44) and (45) determine the mixture of corundum and gehlenite in a thermodynamic equilibrium state. An inspection of Figs. 9 and 10 shows that the condensation of aluminium into corundum is nearly complete where conversion of corundum into gehlenite is thermodynamically favourable.

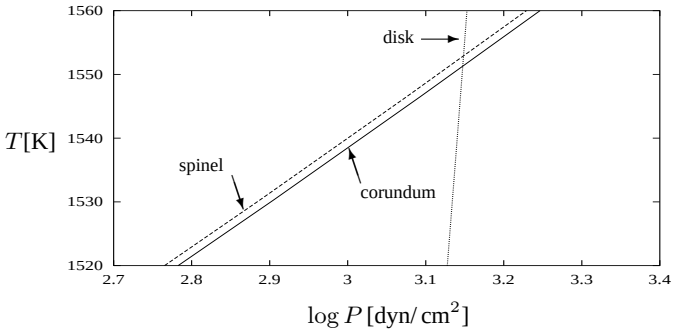

Fig. 12. Equilibrium curves for the conversion of corundum (Al_2O_3) into spinel ($MgAl_2O_4$). The dashed line shows the upper stability limit of spinel, the full line the lower stability limit of corundum. The dotted line shows the pressure-temperature stratification in the midplane of the accretion disk model.

5.3. Spinel

Next we consider the condensation or disappearance of spinel ($MgAl_2O_4$). First we consider the hypothetical case that no other aluminium condensate than spinel is present. Since the Mg required for the formation of spinel is present in the gas phase as the free atom, we consider the reaction

$$\mathrm{Mg} \,+\, 2\mathrm{Al} \,+\, 4\mathrm{H_2O} \,\longrightarrow\, \mathrm{MgAl_2O_4(s)} \,+\, 4\mathrm{H_2}\,. \qquad (46)$$

In thermodynamic equilibrium between the solid and the gas phase species we have

$$\frac{p_{\mathrm{H_2}}^4}{p_{\mathrm{Mg}}\, p_{\mathrm{Al}}^2\, p_{\mathrm{H_2O}}^4} = \mathrm{e}^{-\Delta G/RT} = K_p(T) \qquad (47)$$

where $\Delta G = \Delta G(\mathrm{MgAl_2O_4(s)}) + 4\Delta G(\mathrm{H_2}) - \Delta G(\mathrm{Mg}) - 2\Delta G(\mathrm{Al}) - 4\Delta G(\mathrm{H_2O})$. If f denotes the fraction of the aluminium condensed into spinel, the particle densities of the relevant gas phase species are $p_{\mathrm{Mg}} = (\epsilon_{\mathrm{Mg}} - \frac{1}{2} f\epsilon_{\mathrm{Al}})\, P_{\mathrm{H}}$, $p_{\mathrm{Al}} = (1-f)\,\epsilon_{\mathrm{Al}}\, P_{\mathrm{H}}$ and $p_{\mathrm{H_2O}} = (\epsilon_{\mathrm{O}} - \epsilon_{\mathrm{C}} - \epsilon_{\mathrm{Si}} - 2f\epsilon_{\mathrm{Al}})\, P_{\mathrm{H}}$. We obtain from (47)

$$P^3 = \frac{(1+2\epsilon_{\mathrm{He}})^3\, K_p^{-1}(T)}{2^7(\epsilon_{\mathrm{Mg}} - \frac{1}{2} f\epsilon_{\mathrm{Al}})\,(1-f)^2\,\epsilon_{\mathrm{Al}}^2\,(\epsilon_{\mathrm{O}} - \epsilon_{\mathrm{C}} - \epsilon_{\mathrm{Si}} - 2f\epsilon_{\mathrm{Al}})^4}\,. \qquad (48)$$

$f = 0$ defines the upper limit curve of stability of spinel in the P-T plane. This stability limit is shown in Fig. 9 which also shows the stability limit of the corundum.

Since the stability limit for formation of spinel from gas phase species occurs at a somewhat lower temperature than that for formation of corundum, the formation or disappearance of spinel does not occur by chemisputtering in a reaction like (46) but by conversion of corundum into spinel or vice versa. A possible reaction for this process is

$$\mathrm{Al_2O_3(s)} \,+\, \mathrm{Mg} \,+\, \mathrm{H_2O} \,\longrightarrow\, \mathrm{MgAl_2O_4(s)} \,+\, \mathrm{H_2}\,.$$

In thermodynamic equilibrium between corundum, spinel and the species in the gas phase we have for the partial pressures of the molecules

$$\frac{p_{\mathrm{H_2}}}{p_{\mathrm{Mg}}\, p_{\mathrm{H_2O}}} = \mathrm{e}^{-\Delta G/RT} = K_x(T) \qquad (49)$$

where $\Delta G = \Delta G(\mathrm{MgAl_2O_4}) + \Delta G(\mathrm{H_2}) - \Delta G(\mathrm{Al_2O_3}) - \Delta G(\mathrm{Mg}) - \Delta G(\mathrm{H_2O})$. Assume that a fraction f of the aluminium first is condensed into corundum and that a fraction x of this is converted into spinel. The partial pressures of the gas phase species are $p_{\mathrm{Mg}} = (\epsilon_{\mathrm{Mg}} - \frac{1}{2}(1-x) f\epsilon_{\mathrm{Al}})\, P_{\mathrm{H}}$ and $p_{\mathrm{H_2O}} = \left(\epsilon_{\mathrm{O}} - \epsilon_{\mathrm{C}} - \epsilon_{\mathrm{Si}} - [\frac{3}{2}(1-x) + 2x] f\epsilon_{\mathrm{Al}}\right)\, P_{\mathrm{H}}$. We obtain from (49)

$$P = \frac{(1+2\epsilon_{\mathrm{He}})}{4\,(\epsilon_{\mathrm{Mg}} - \frac{1-x}{2} f\epsilon_{\mathrm{Al}})\,\left(\epsilon_{\mathrm{O}} - \epsilon_{\mathrm{C}} - \epsilon_{\mathrm{Si}} - \frac{3+x}{2} f\epsilon_{\mathrm{Al}}\right)\, K_x(T)}\,. \qquad (50)$$

This equation and Eq. (40) which reads in the present case as

$$P^2 = \frac{(1+2\epsilon_{\mathrm{He}})^2}{2^5\,(1-f)^2\,\epsilon_{\mathrm{Al}}^2\,(\epsilon_{\mathrm{O}} - \epsilon_{\mathrm{C}} - \epsilon_{\mathrm{Si}} - \frac{3+x}{2} f\epsilon_{\mathrm{Al}})^3\, K_p(T)}\,, \qquad (51)$$

for given T form a system of two equations for the three unknown quantities P, f, and x. They determine, thus, for fixed f or x a family of curves of constant f or x in the P-T plane.

For solar system element composition the aluminium abundance is of the order of 1% of the oxygen abundance. Thus we may neglect with an accuracy sufficient for our purposes ϵ_{Al} compared to ϵ_{O}. Squaring (50) and equating this to (51) yields

$$f = \frac{\epsilon_{\mathrm{Al}}\sqrt{2(\epsilon_{\mathrm{O}} - \epsilon_{\mathrm{C}} - \epsilon_{\mathrm{Si}})\frac{K_p(T)}{K_x^2(T)}} - \epsilon_{\mathrm{Mg}}}{\epsilon_{\mathrm{Al}}\sqrt{2(\epsilon_{\mathrm{O}} - \epsilon_{\mathrm{C}} - \epsilon_{\mathrm{Si}})\frac{K_p(T)}{K_x^2(T)}} - \frac{1-x}{2}\epsilon_{\mathrm{Al}}}\,. \qquad (52)$$

This determines f in terms of x or vice versa. The result can be used in (50) to determine the total pressure P.

We assume x to be held constant. The curve defined in the P-T plane by letting $x = 0$ is the limit curve above and to the left of which no spinel exist in an equilibrium state in the presence of corundum. A second curve defined in the P-T plane by letting $x = 1$ is the limit curve below and to the right of which no corundum exists in an equilibrium state in the presence of spinel. Between these two limit curves, if they exist[2], corundum and spinel coexist in thermodynamical equilibrium. Fig. 12 shows this two limit curves calculated from Eq. (52). The transition from spinel to corundum occurs in a narrow temperature interval of the order of only 1 K, i.e. the transition between both solids is nearly discontinuous in temperature.

The limit for conversion of spinel into corundum also is shown in Fig. 9. This limit occurs at a much lower temperature than the limit for conversion of spinel into gas phase molecules. Spinel does not disappear by chemisputtering in a reaction like (47) but by conversion into corundum. This conversion also occurs at a lower temperature than that where corundum is partly converted into gehlenite. Thus, some fraction of the aluminium is bound in gehlenite at the limit where spinel is converted into

[2] This depends on the element abundances. With much more Mg than Al, both limit curves do exist but if Mg would be much less abundant than Al a complete conversion of corundum into spinel would be impossible.

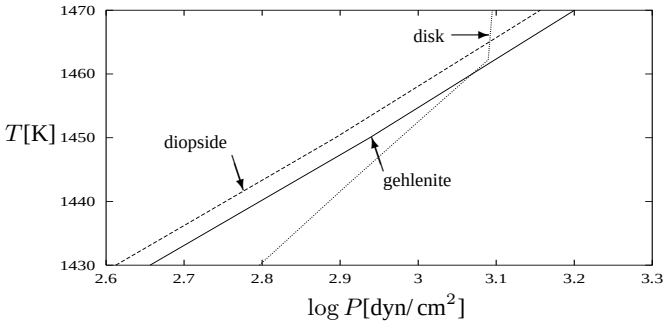

Fig. 13. Equilibrium curves for the conversion of melilite ($Al_2Ca_2SiO_7$) into diopside ($CaMgSi_2O_6$) and spinel ($MgAl_2O_4$). The dashed line shows the upper stability limit of diopside, the full line the lower stability limit of gehlenite. The dotted line shows the pressure-temperature stratification in the midplane of the accretion disk model. The inflection in this line corresponds to the stability limit of iron.

corundum. The lower stability limit of corundum then is obtained if we let $x = 1$ in Eq. (50). This together with Eqs. (44) and (45) then determines the degree g of condensation of calcium in gehlenite and the fraction f of aluminium in corundum resp. in spinel at the border between the region of existence between these two compounds.

5.4. Diopside

The calcium bound in gehlenite ($Al_2Ca_2SiO_7$) at lower temperatures tends to be bound more stable in diopside ($CaMgSi_2O_6$). The aluminium liberated in the conversion of gehlenite to diopside does not appear as a gas phase species but forms a solid. Since gehlenite coexists with spinel in the relevant temperature regime, the aluminium content of the gehlenite forms spinel. The magnesium required for this is present as free atoms in the gas phase and the additional silicon and oxygen required to form diopside is present as SiO and H_2O molecules. A possible reaction for the conversion of gehlenite into diopside then is

$$\mathrm{Al_2Ca_2SiO_7(s)} + 3\mathrm{Mg} + 3\mathrm{SiO} + 6\mathrm{H_2O} \longrightarrow 2\mathrm{CaMgSi_2O_6(s)} + \mathrm{MgAl_2O_4} + 6\mathrm{H_2}\,.$$

In chemical equilibrium the gas phase species satisfy the relation

$$\frac{p_{\mathrm{H_2}}^6}{p_{\mathrm{Mg}}^3\, p_{\mathrm{SiO}}^3\, p_{\mathrm{H_2O}}^6} = \mathrm{e}^{-\Delta G/RT} = K_p(T) \qquad (53)$$

where $\Delta G = 2\Delta G(\mathrm{diop.}) + 2\Delta G(\mathrm{spin.}) + 6\Delta G(\mathrm{H_2}) - \Delta G(\mathrm{geh.}) - 3\Delta G(\mathrm{Mg}) - 3\Delta G(\mathrm{SiO}) - 6\Delta G(\mathrm{H_2O})$. If f denotes the fraction of the calcium bound in diopside and if the only other abundant calcium compound is gehlenite, then the partial pressure of magnesium atoms in the gas phase is $p_{\mathrm{Mg}} = \left(\epsilon_{\mathrm{Mg}} - f\epsilon_{\mathrm{Ca}} - \frac{1}{2}\left(\epsilon_{\mathrm{Al}} - (1-f)\epsilon_{\mathrm{Ca}}\right)\right) P_{\mathrm{H}}$ since the calcium either is bound in diopside or gehlenite and the aluminium is bound either in gehlenite or spinel. The partial pressures of SiO and H_2O are $p_{\mathrm{SiO}} = \left(\epsilon_{\mathrm{Si}} - 2f - \frac{1}{2}(1-f)\epsilon_{\mathrm{Ca}}\right) P_{\mathrm{H}}$ and $p_{\mathrm{H_2O}} = \left(\epsilon_{\mathrm{O}} - \epsilon_{\mathrm{C}} - \epsilon_{\mathrm{Si}} - 4f\epsilon_{\mathrm{Ca}} - 3(1-f)\epsilon_{\mathrm{Ca}}\right) P_{\mathrm{H}}$. From the law of mass action (53) we obtain

$$P^6 = \frac{(1+2\epsilon_{\mathrm{He}})^6}{2^{12}\left(\epsilon_{\mathrm{Mg}} - \frac{3f-1}{2}\epsilon_{\mathrm{Ca}} - \frac{1}{2}\epsilon_{\mathrm{Al}}\right)^3\left(\epsilon_{\mathrm{Si}} - \frac{3f+1}{2}\epsilon_{\mathrm{Ca}}\right)^3} \cdot \frac{1}{\left(\epsilon_{\mathrm{O}} - \epsilon_{\mathrm{C}} - \epsilon_{\mathrm{Si}} - (3+f)\epsilon_{\mathrm{Ca}} - 2\epsilon_{\mathrm{Al}}\right)^6 K_p(T)}\,. \qquad (54)$$

This defines the curve in the P-T plane along which the fraction f of the calcium is bound in diopside while the remaining fraction of the Ca is bound in gehlenite. At the same time the Al not bound in gehlenite is bound in spinel. $f = 0$ defines the upper stability limit of diopside above and to the left of which no diopside exists while $f = 1$ defines the lower stability limit of gehlenite below and to the right of which no gehlenite exists[3]. These two limit curves are shown in Fig. 13. The transition between the two extreme cases occurs within a very narrow temperature interval of only a few degree where both solids coexist. The transition between the two Ca bearing compounds occurs nearly discontinuous at a sharp transition temperature.

The limit for conversion of gehlenite into diopside also is shown in Fig. 9 from which one easely recognises that the limit occurs at nearly the same temperature but always slightly above that where forsterite starts to be formed with decreasing temperature. This justifies our previous assumption that most of the Mg is present as free atoms in the gas phase where the transition between gehlenite and diopside occurs.

5.5. Anorthite

The aluminium bound in spinel according to calculations of cooling sequences (cf. Grossman 1972, Lattimer et al. 1978) tends to form at lower temperatures the more stable aluminium–calcium compound anorthite ($CaAl_2Si_2O_8$). A conversion of the spinel into anorthite is possible only if the calcium required to form anorthite is taken from diopside which is the only abundant calcium bearing compound. The excess silicon liberated in the destruction of the diopside then will form at the relevant temperatures the magnesium silicate forsterite. A possible reaction for the conversion of spinel and diopside into anorthite and forsterite is

$$\mathrm{MgAl_2O_4(s)} + \mathrm{CaMgSi_2O_6(s)} + \mathrm{H_2O} + \mathrm{SiO} \longrightarrow \mathrm{CaAl_2Si_2O_8(s)} + \mathrm{Mg_2SiO_4(s)} + \mathrm{H_2}\,. \qquad (55)$$

The additional oxygen and silicon atoms required for the conversion are available from H_2O and SiO molecules from the gas phase. If f denotes the fraction of the aluminium bound in anorthite and g the fraction of the silicon bound in forsterite, the partial pressures of H_2O and SiO in the gas phase are $p_{\mathrm{H_2O}} = \left[\epsilon_{\mathrm{O}} - \epsilon_{\mathrm{C}} - (1+3g)\epsilon_{\mathrm{Si}} - (2-f)\epsilon_{\mathrm{Al}} - 6\epsilon_{\mathrm{Ca}}\right] P_{\mathrm{H}}$ and $p_{\mathrm{SiO}} = \left[(1-g)\epsilon_{\mathrm{Si}} - 2\epsilon_{\mathrm{Ca}}\right] P_{\mathrm{H}}$ since the Ca either is bound in diopside or in anorthite and since the aluminium either is bound in spinel or in anorthite. According to the law of mass action the

[3] The upper stability limit of gehlenite is determined by Eq. 44

partial pressures of the gas phase species involved in reaction (55) in chemical equilibrium satisfy the relation

$$\frac{p_{\rm H_2}}{p_{\rm H_2O}\,p_{\rm SiO}} = {\rm e}^{-\Delta G/RT} = K_p(T) \tag{56}$$

where $\Delta G = \Delta G({\rm anor.}) + \Delta G({\rm for.}) + \Delta G({\rm H_2}) - \Delta G({\rm spin.}) - \Delta G({\rm diop.}) - \Delta G({\rm H_2O}) - \Delta G({\rm SiO})$. It follows from Eq. (56)

$$P = \frac{1+2\epsilon_{\rm He}}{4(\epsilon_{\rm O}-\epsilon_{\rm C}-(1+3g)\epsilon_{\rm Si}-(2-f)\epsilon_{\rm Al}-6\epsilon_{\rm Ca})} \cdot \frac{1}{((1-g)\epsilon_{\rm Si}-2\epsilon_{\rm Ca})\;K_p(T)}\,. \tag{57}$$

On the other hand, the fraction g of the silicon condensed into forsterite is determined by (18) which reads in the present case as

$$P^3 = \frac{(1+2\epsilon_{\rm He})^3}{2^6\,((1-g)\epsilon_{\rm Si}-2\epsilon_{\rm Ca})\;(\epsilon_{\rm Mg}-2g\epsilon_{\rm Si}-\epsilon_{\rm Ca}+\frac{2f-1}{2}\epsilon_{\rm Al})^2} \cdot \frac{1}{(\epsilon_{\rm O}-\epsilon_{\rm C}-(1+3g)\epsilon_{\rm Si}-(2-f)\epsilon_{\rm Al}-6\epsilon_{\rm Ca})^3\,K_{p,{\rm for}}(T)}\,. \tag{58}$$

Combining both equations for P yields an equation for f and g which can be solved for g with the result

$$g = \frac{W\left(\epsilon_{\rm Mg}-\epsilon_{\rm Ca}+\frac{2f-1}{2}\epsilon_{\rm Al}\right)+2\epsilon_{\rm Ca}-\epsilon_{\rm Si}}{(2W-1)\,\epsilon_{\rm Si}} \tag{59}$$

where

$$W = [K_{p,{\rm for.}}(T)]^{\frac{1}{2}}\;\left[K^3_{p,{\rm anor.}}(T)\right]^{-\frac{1}{2}}\,. \tag{60}$$

$f=0$ defines the upper stability limit of anorthite while $f=1$ the defines the lower stability limit of spinel where the Al contained in spinel is completely consumed in the formation of anorthite. Fig. 9 shows the result for f. In accord with the finding of Sharp & Huebner (1990) that anorthite does not form in their calculation at temperatures above $\approx 1\,000$ K the conversion of spinel into anorthite occurs only at rather low temperatures. We do not consider this compound further since it is not present in the inner region of the accretion disk where the silicates and the aluminium compounds are destroyed.

5.6. Aluminium compounds in the disk

According to our above findings the following aluminium compounds are formed in chemical equilibrium in the order of increasing temperature:

1. Anorthite and Diopside. At low temperatures the anorthite consumes all of the available aluminium. Since anorthite contains two Al atoms for each Ca atom and since the Ca abundance exceeds one half of the aluminium abundance, the excess of Ca forms diopside.
2. Spinel and Diopside. As the temperature increases the anorthite is converted at a specific temperature into spinel. The spinel then consumes all of the available aluminium. Since spinel contains no Ca, the Ca liberated in the conversion of anorthite into spinel also forms diopside. Thus all of the Ca then is bound in diopside.
3. Spinel and gehlenite. As the temperature increases further the diopside is converted into gehlenite at a specific temperature. The gehlenite then consumes all of the available Ca and a corresponding amount of the aluminium. Only the excess of the Al over Ca remains to be bound in spinel.
4. Gehlenite and corundum. With increasing temperature the spinel is converted into corundum at a specific temperature. At this point of conversion of spinel into corundum, the gehlenite consumes all the available Ca. With increasing temperature, however, the fraction of the Ca bound in gehlenite steadily decreases while the fraction of the Al bound in corundum correspondingly increases.
5. Corundum. At a certain temperature the gehlenite disappears. The corundum then consumes all of the available Al. With continued increase of the temperature the fraction of the Al bound in corundum steadily decreases while the fraction of the Al remainig in the gas phase correspondingly increases. At a specific temperature the last corundum disappears. Beyond that temperature no solid aluminium compunds exist in the disk.

As our discussion of the equilibrium abundances of aluminium compounds shows, this sequence of events occurs in any environment where the pressure and temperature monotonuously increase. Only the precise values of the temperature where the different aluminium compounds appear or disappear depend on the details of the P-T stratification in the accretion disk.

6. Model calculation for a protoplanetary disk

6.1. Equations for the disk structure

The calculation of the structure of a protoplanetary accretion disk is based on the semi-analytical model for a thin stationary accretion disk of Duschl et al. (1996)[4]. The details of the approximations on which this model is based on are described there. The resulting basic equations for the disk structure are

$$\Sigma = 2500\;\frac{\rm g}{\rm cm^2}\;s^{-\frac{3}{5}} \tag{61}$$

$$h = 1.446\cdot 10^{12}\;{\rm cm}\;s^{\frac{21}{20}}\;M^{-\frac{3}{8}}\left(\dot{\mathbf{M}}_{-7}\,\kappa\right)^{\frac{1}{8}}\;\mu^{-\frac{1}{2}} \tag{62}$$

$$T = 997\;{\rm K}\;s^{-\frac{9}{10}}\;M^{\frac{1}{4}}\left(\dot{\mathbf{M}}_{-7}\,\kappa\right)^{\frac{1}{4}} \tag{63}$$

$$P = 71.65\;\frac{\rm g}{\rm cm\;s^2}\;s^{-\frac{51}{20}}\;M^{\frac{5}{8}}\left(\dot{\mathbf{M}}_{-7}\kappa\right)^{\frac{1}{8}}\;\mu^{-\frac{1}{2}} \tag{64}$$

[4] In the printed version of this paper the dot over $\dot{M}$ denoting the mass-loss rate is missing in all equations. The correct version may be obtained from the WWW-page of the Institute of Theoretical Astrophysics, Heidelberg

Table 2. Model parameters of the accretion disk used in the computation of disk structure

mass M	$1\,M_\odot$
mass-loss rate $\dot{\mathbf{M}}$	$10^{-7}\,M_\odot/\mathrm{yr}$
surface density Σ	2500 g·cm^{-2} at $s=1$

where s is the radial distance from the protosun in units AU, Σ is the surface density, h the (half) thickness of the disk, M the mass of the protostar in solar masses, $\dot{\mathbf{M}}_{-7}$ the constant accretion rate in units of $10^{-7}\,M_\odot/\,\mathrm{yr}$, and P and T are the pressure and temperature in the midplane of the disk, respectively. κ is the Rosseland mean mass extinction coefficient and μ the mean molecular weight. The opacity is determined by the opacity of the dust and the gas. The approximation for κ due to dust used in the model calculation is described below. The opacity of the gas component is calculated from the analytical approximations given by Bell & Lin (1994). The details of the approximation of the gas opacity as used in this model calculation are described in Finocchi et al. (1997). The basic parameters of the disk used for the model calculation are listed in Tab. 2.

The inwards directed drift velocity of the disk material is

$$v_s = 26.94\,\frac{\mathrm{cm}}{\mathrm{s}}\,s^{-\frac{2}{5}}\,\dot{\mathbf{M}}_{-7}\,. \tag{65}$$

The characteristic timescale for a significant change in temperature follows from (63) and (65) as

$$\tau_T = \frac{T}{v_s}\left|\frac{\mathrm{d}T}{\mathrm{d}t}\right|^{-1} = 6.19\cdot 10^{11}\ \mathrm{s}\ s^{\frac{7}{5}}\dot{\mathbf{M}}_{-7}^{-1}\,. \tag{66}$$

(see Fig. 1). This corresponds to the characteristic timescale for temperature changes experienced by a dust grain as it spirals inwards with a radial drift velocity component given by (65).

6.2. Absorption by dust grains

The disk structure depends strongly on the mass extinction coefficient κ of the disk material. Throughout most part of the accretion disk the opacity is dominated by the strong absorption and scattering by the dust grains. As we have seen above, there exist many different kinds of dust species in different parts of the accretion disk, depending on the local pressure and temperature conditions. At least the contribution of the most abundant of the various species to the total opacity has to be considered in a model calculation of the disk structure. The dust mixture used in this calculation is that of the P94 model of Pollack et al. (1994) as specified in Sect. 2 and the mixture of aluminium compounds predicted from chemical equilibrium calculations at temperatures where silicate and iron grains are already destroyed.

The composition of the P94 dust mixture does not correspond to the mixture obtained by any thermodynamic equilibrium composition at some pressure P and temperature T. It results from contributions from various sources, stellar and interstellar ones, where it is believed to be formed under extreme non-equilibrium conditions. The mixture will be subject to changes in the relative fraction of its constituents as the inwards drifting disk material gradually becomes warmer. This has to be considered in calculating the dust opacity.

In calculating the opacity of the dust we do not consider the full set of dust components existing in the disk but only the following four species:

1. The astronomical silicate as defined in the model of Draine & Lee (1984). The complex index of refraction given by Draine (1985) is used for calculating the extinction by the silicate dust components of the P94 dust mixture in the cold parts of the accretion disk ($T \lesssim 800\,\mathrm{K}$) where annealing of the disordered lattice structure of interstellar dust is inefficient. We prefer this over the silicate absorption data used by Pollak et al. (1994) since in the mid infrared the data of Draine seem to give the best representation of dust extinction (e.g. Mathis 1996, Li & Greenberg 1997) and it is the opacity in this spectral region that determines the disk structure between the region of ice vapourisation and annealing of the amorphous silicate dust.
2. Olivine as a model for a silicate with a well ordered lattice structure. We do not discriminate in our extinction calculation between the two abundant silicate species olivine and orthopyroxene since both have a rather similar complex dielectric coefficient (cf. Fig. 1 of Pollack et al. 1994 for instance) and take olivine as being representative for both materials. The olivine is used for calculating the extinction by silicates after annealing took place. Data for the complex index of refraction of crystalline olivine in the wavelength region $80\,\text{Å} \leq \lambda \leq 250\,\mu$m have been obtained several years ago from D.R. Huffman (private communication, c.f. also Huffman & Stapp 1973)). The crystalline olivine shows a much smaller absorption than the "dirty astronomical silicate" of Draine (1984) or the glassy olivine studied by Dorschner et al. (1995).
3. Iron metal. For the wavelength region $\lambda \leq 12.4\,\mu$m we use data for the complex index of refraction as given in the CRC handbook (Lide 1995). For longer wavelength we use the same data as Pollak et al. (1994).
4. Corundum is chosen as a representative absorber for the aluminium compounds. We do not discriminate in our calculation of the extinction between the different aluminium dust species but treat them all as being corundum. Data for the complex index of refraction of corundum are taken from Koike et al. (1995). We use their ISAS-data representing the absorption properties of fine corundum grains produced by combustion of solid-rocket propellants. We believe that the formation conditions of such grains are roughly comparable to a corundum condensate formed in circumstellar shells.

In our present model calculation we do not consider the carbon dust component since we have not included the complex chemistry of carbon dust destruction (see Finocchi et al. 1997) in this model calculation. The troilite dust component of the P94 dust mixture is neglected in our calculation of the dust opacity, since

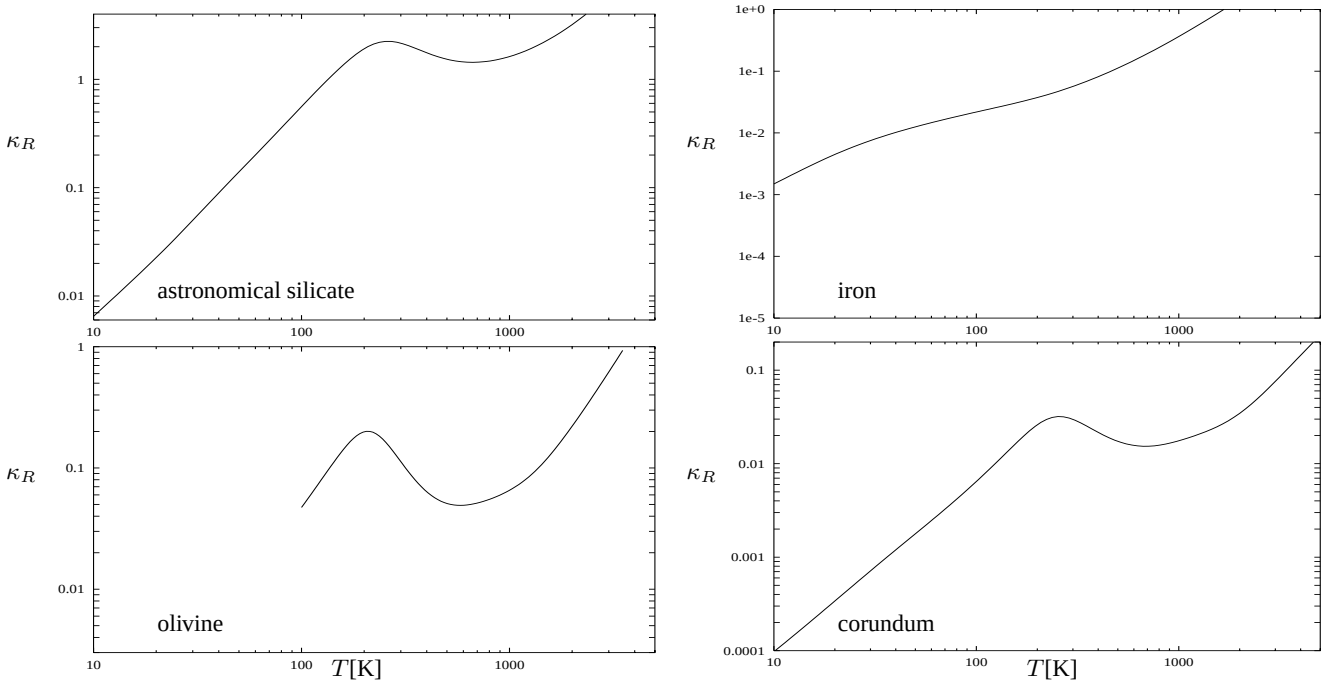

Fig. 14. Rosseland mean κ_R of the mass extinction coefficient (in units cm^2/g) averaged with a MRN size distribution for some important dust species

this species is only a minor absorber (eg. Pollack et al. 1994). It is simply treated as being iron in the opacity calculation. The SiO_2 dust component assumed to be present in the P94 dust mixture is treated in the opacity calculation as being a silicate.

Real iron grains in an accretion disk are not really pure iron particles but their material is a solid solution of iron with an admixture of several percent of nickel and small contents of some other elements. This is not considered in our calculations of the opacity of such grains. Further we do not consider that after annealing of the dirty astronomical silicate the crystalline silicate grains resulting from this may contain tiny inclusions of for instance iron grains or of aluminium-calcium compounds.

The Rosseland mean opacities of these four dust materials was calculated as follows: For a dense grid of particle radii a and frequencies ν the extinction coefficient was calculated by Mie theory for spherical grains for each a and ν. The complex index of refraction for the dust materials was chosen as discussed above. The reciprocal κ's first are integrated numerically over the paricle size distribution and the result is used to calculate the Rosseland mean opacities κ_R by a numerical integration according to the standard definition of κ_R. The results are shown in Fig. 14. We assumed in this calculation that the dust grains are distributed in size between $0.005\,\mu$ and $0.25\,\mu$m according to the widely accepted Mathis-Rumpl-Nordsiek (MRN) size distribution (Mathis et al. 1977). This is a reasonable assumption for the silicate dust grains since the MRN radius spectrum is assumed to describe well the size of interstellar grains. Though one expects that grains in the cold outer part of the accretion disk have agglomerated into bigger sized clusters of particles (Stognienko et al. 1995), these agglomerates are bound only by weak van der Waals forces. They are expected to disintegrate again in the warm parts of the accretion disk (T at least several 100 K), in which we are interested in this paper. More recent models for interstellar dust absorption favour a different distribution of grain sizes for the silicate grain component of the dust mixture (Li & Greenberg 1997) or for all components (Mathis 1996). Since the dust grains prior to the onset of planetesimal formation all are small compared to the wavelengths of interest even in the warm parts of the accretion disk, the extinction does not depend on the special choice of the size distribution of grains. In the cold part of the accretion disk, however, the grains are likely to have a porous fluffy structure and the extinction then depends on the size and structure of the dust aggregates (Miyake & Nakagawa 1993, Stognienko et al. 1995).

For the iron and the aluminium dust component the assumption of a MRN distribution is rather arbitrary. It is used in default of any information on the real sizes of such grains.

As can be seen from Fig. 14 the most efficient absorber in the inner parts of the accretion disk is the "dirty astronomical silicate". It dominates the opacity of the disk matter until it is converted into crystalline silicate due to annealing at elevated temperatures (see below). After annealing of the amorphous silicate dust the opacity is dominated by the opacity of the iron grains which are more efficient absorbers than the crystalline silicates. Once the iron grains are vapourised the extinction is dominated by the aluminium compounds until also these grains are destroyed close to the star. The disappearance of certain dust materials with increasing temperature obviously is accompanied at each step by a strong decrease of the extinction coefficient.

This has strong implications for the structure of the accretion disk, as we shall see in Sect. 8.

7. Annealing and diffusion II

The silicate dust grains exist in the accretion disk in at least three different modifications: (i) As the grains enter the accretion disk from the parent molecular cloud they have most likely an amorphous lattice structure. The P94 model assumes a mixture of silicate compounds as specified in Tab. 1. (ii) The components of this mixture are thermochemically unstable in the warm inner parts of the accretion disk. The most stable condensed silicate compounds in an environment with solar system composition are enstatite with a very low iron content and (iii) above the stability limit of the enstatite grains, an iron-poor olivine with nearly the composition of forsterite is the thermodynamically most stable silicate compound. Thus, if the disk material drifts inwards we expect that with increasing temperature first internal annealing processes convert the grains from an amorphous to a crystalline structure (see Sect. 3). Impurities which do not solve in the silicate crystal assemble most likely in localised inclusions within the polycrystalline material and may crystallise into small particulates of a different chemical composition within the bigger silicate grains. This especially is expected to occur for the iron of which only as small fraction is incorporated into the orthopyroxene and olivine grains in chemical equilibrium at temperatures above 800 K (Saxena & Ericksson 1986). If the internal structure changes to that of enstatite the excess of the iron content of silicates in the P94 mixture over the equilibrium concentration most likely assembles in small iron inclusions within the polycrystalline material. Also complete removing of the Fe by diffusion to the surface and loss to the gas phase may occur at sufficiently high temperature during complete crystallisation of the grain.

At a temperature of roughly 1 200 K the conversion of enstatite to forsterite becomes thermodynamically favourable (cf. Fig. 8). Finally the forsterite grains are destroyed when the disk matter crosses the stability limit of forsterite. Any silicate grain, thus, suffer the following sequence of transmutations on its outside-in journey in the disk:

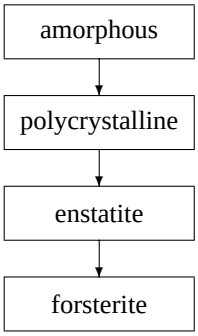

In the annealing experiment of Nuth & Donn (1982) it was found that forsterite forms from an amorphous silicate smoke by annealing for up to 30 hours at 1 000 K, but not enstatite, though the enstatite is the thermodynamically favoured compound. Thus, possibly the forsterite grain component in the initial P94 mixture cannot easely be converted into enstatite by solid state annealing and retains its initial composition until it is destroyed in the inner part of the disk. Also the enstatite grain component in the P94 mixture may be not easely converted into forsterite in the region where forsterite is thermodynamically more stable than enstatite and survives until it is destroyed. In this paper we shall assume that the conversion occurs with a sufficiently small timescale compared to the characteristic timescale of $\gtrsim 10^4$ yrs for temperature changes such that the relative fractions of forsterite and enstatite always correspond to the chemical equilibrium state.

With respect to the disk structure the most important of these changes of dust properties is the transition from amorphous to polycrystalline dust since this is accompanied by a considerable change in the absorption properties of the dominant absorber, as can be seen from Fig. 14. In order to account for this process in a model calculation for the disk structure we consider the following crude model for the annealing process by internal hopping and re-arrangement processes: We assume that there exist certain tiny islands of a few geometrically well ordered SiO_4 tetrahedrons within the random network of SiO_4 groups of the amorphous dust, which serve as "growth centres" for the formation of an ordered lattice structure. Once some SiO_4 tetrahedron from the random network adjacent to such a growth center has re-arranged its position and orientation relative to the growth center by internal hopping such that it now fits well to the structure of the growth centre it finds itself in a deeper local minimum of the lattice potential than in its previous position (orientation). It is, then, much more likely that the next adjacent tetrahedron aligns to the growth center as that the former SiO_4 group gives up its energetically favourable state. The growth centre then has increased in size by one building block of the lattice. We then assume that the conversion of the amorphous dust material into a polycrystalline material occurs by growth of the well ordered region into its disordered environment, starting at some tiny well ordered centres which always exist in a disordered material.

Let V_0 be the volume occupied by a single building block of the lattice and let V be the actual volume of a growth centre. The increase of V per unit time is given by

$$\frac{\mathrm{d}V}{\mathrm{d}t} = V_0 \cdot 6 \left(\frac{V}{V_0}\right)^{\frac{2}{3}} \cdot \nu\, \mathrm{e}^{-T_0/T} \,. \tag{67}$$

$6(V/V_0)^{2/3}$ is the number of surface sites of the growth centre (which we take for simplicity to be a cube) where a new building block can be added from the environment. ν is the frequency of attempts of particles from the environment to jump into an energetically more favourable state by aligning to the surface of the growth centre and kT_0 is the activation energy barrier to be surmounted in a successful transition. For ν and T_0 we use the values given in Sect. 3 for annealing of amorphous silicates.

Eq. (67) integrates to

$$V^{\frac{1}{3}} = 2V_0^{\frac{1}{3}}\, \nu \int_0^t dt'\, \mathrm{e}^{-T_0/T(t')} \,. \tag{68}$$

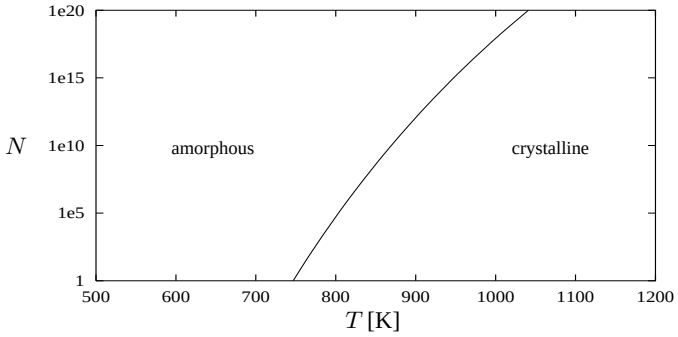

Fig. 15. Number N of building blocks of the silicate lattice contained in one growth centre if the dust temperature has increased to the temperature T.

Since the integrand is steeply increasing near the upper limit of integration, we can expand the exponent around $t' = t$

$$\frac{T_0}{T(t')} \approx \frac{T_0}{T(t)} - \frac{T_0}{T^2(t)} \frac{\mathrm{d}T}{\mathrm{d}t} (t' - t)$$

and then integrate with the result

$$\begin{aligned} V^{\frac{1}{3}} =& 2V_0^{\frac{1}{3}} \, \nu \, \mathrm{e}^{-T_0/T(t)} \, \frac{T^2}{T_0} \frac{\mathrm{d}t}{\mathrm{d}T} \\ =& 2V_0^{\frac{1}{3}} \, \nu \, \mathrm{e}^{-T_0/T(t)} \, \frac{T^2}{T_0} \frac{\mathrm{d}s}{\mathrm{d}T} \, v_s^{-1} \, . \end{aligned} \tag{69}$$

In Fig. 15 we show the number $N = V/V_0$ of building blocks contained in one growth centre as a function of the temperature in the central plane of the disk. dT/ds and v_s are calculated in this case from the equations for the disk structure with the simple assumption of $\kappa = 1\,\mathrm{cm}^2/\mathrm{g}$. If we arbitrarily assume that we have initially one growth center per 10^5 Si atoms in the dust material we find a temperature of $\approx 800\,\mathrm{K}$ for the transition from an amorphous to a polycrystalline structure. This agrees with our previous estimate in Sect. 3 since a $0.01\,\mu$ silicate grain contains roughly 10^5 Si atoms. Due to the steep increase of V with T our estimate of the transition temperature is rather robust and depends only weakly on the precise number of growth centers which are really present in the dust material.

As a crude measure for the degree of conversion of the amorphous into polycrystalline grains we introduce the ratio of the total volume of all growth centres to the total volume of all silicate grains

$$f_{\mathrm{cr}} = \min \left(1, \frac{V_{\mathrm{centres}}}{V_{\mathrm{silicates}}} \right) \, .$$

We do not discriminate between the different silicate dust components in the P94 mixture. The total volume of all centres is $x \epsilon_{\mathrm{Si}} n_{\mathrm{H}} \cdot V(t)$ where x the concentration of growth centres per Si nuclei which we choose to be $x = 10^{-5}$ and n_{H} is the density of hydrogen nuclei. The total volume of all silicates is given by $\epsilon_{\mathrm{Si}} n_{\mathrm{H}} \cdot V_0$. It follows from (69) and the disk equations

$$\begin{aligned} f_{\mathrm{cr}} =& \frac{xV(t)}{V_0} = x \left[2 \, \nu \, \mathrm{e}^{-T_0/T(t)} \, \frac{T^2}{T_0} \frac{\mathrm{d}s}{\mathrm{d}T} \, v_s^{-1} \right]^3 \\ =& 2.17 \, 10^{71} \, T^{-\frac{5}{3}} \, \mathrm{e}^{-123000/T} \, M^{-\frac{5}{6}} \, \dot{\mathbf{M}}_{-7}^{-\frac{59}{18}} \, \kappa^{-\frac{5}{6}} \end{aligned} \tag{70}$$

If the calculated value of f_{cr} exceeds unity we have to put $f_{\mathrm{cr}} = 1$.

The pressure at the transition point is approximately $50\,\mathrm{dyn}/\,\mathrm{cm}^2$. In chemical equilibrium at the transition point at this pressure and a temperature of 800 K the orthopyroxene and olivine both are nearly iron free (cf. Figs. 20 and 21 in Saxena & Ericksson 1986 for instance). The transition temperature is well above the temperature for formation of FeS, i.e., the iron is present as the free metal. After annealing the iron content of the silicates in the initial P94 mixture then forms separate iron particulates. Whether they form inclusions inside the silicate grains or whether the excess iron outgasses and precipitates on the iron grains contained in the P94 mixture is an open question which can only be answered by a detailed study of the underlying transport processes which is out of the scope of the present paper.

The steep increase of f_{cr} with T means that the transition from amorphous to polycrystalline grains occurs within a rather narrow temperature interval. This transition has strong implications for the disk structure since during this transition the mass extinction coefficient drops by nearly two decades, as the extinction changes from that of the amorphous silicate to that of a mixture of olivine and iron particles (see Fig. 14). In view of the uncertainties as whether part of the iron partially is included as small inclusions in the silicates or not we calculate the extinction coefficient in the transition region as a simple linear superposition of the contributions of the three main absorbers

$$\begin{aligned} \kappa =& (1 - f_{\mathrm{cr}}) \kappa_{\mathrm{amorphous}} + f_{\mathrm{cr}} \kappa_{\mathrm{olivine}} \\ & + (0.49 + 0.51 \, f_{\mathrm{cr}}) \kappa_{\mathrm{iron}} \, . \end{aligned} \tag{71}$$

The contribution of iron to κ considers that 49% of the iron in the P94 mixture is already present as iron grains in the region of the disk where annealing occurs while 51% is bound in the silicates prior to annealing (see Tab. 1) and has precipitated onto iron grains thereafter.

8. Disk model

Based on the assumptions outlined above a model for a protostellar accretion disk has been calculated assuming a mass of the central star of one solar mass and an accretion rate of $10^{-7} M_{\odot}/\,\mathrm{yr}$. This corresponds to a late stage of the viscous evolution of the accretion disk around a solar type star when the rate of mass infall from the parent molecular cloud has become small and such material is added only to the far outer disk region. Then there develops a nearly stationary state in the inner parts of the accretion disk the structure of which is described by the set of equations of Sect. 6.1.

A model is calculated for the radius regime $40\,\mathrm{AU} \geq s \geq R_*$. The stellar radius R_* is determined by assuming a luminosity of $L_* = 10 L_{\odot}$ and an effective temperature of $T_{\mathrm{eff}} = 4\,500\,\mathrm{K}$ for a newly born star of one solar mass (e.g. Stahler 1983).

First the equations for the stability limits of all dust components important for the opacity have been solved simultaneously with the disk equations to determine the radius where the last grains of these dust components disappear. For instance we

solved Eq. (18) simultaneously with the disk Eqs. (63), (64) to obtain the inner radius where forsterite disappears. This was done for water ice, enstatite, forsterite, iron, and corundum, and for the limit where conversion of the amorphous silicate grains to crystalline silicate grains is completed. For iron and forsterite this is a somewhat delicate problem since both species disappear in the region where the stability limits of both condensates intersect each other and it is not a priori known which one of the two disappears first. We calculated both, the limit of disappearance of silicate assuming that iron disappears first, and vice versa. The result with the higher temperature for destruction of both components is the correct one. In the model based on our above assumptions on the dust opacity the iron survives the forsterite, see Fig. 19, but if the opacity of aluminium compounds would be higher than that one used in the present calculation the forsterite might survive the iron. In all other cases the stability limits of the dominating absorbers are well separated in T and there is no doubt with respect to the order of disapperance of the dust components. The disk equations then where solved in the intervals between the stability limits considering the opacities of all components which do exist in that interval. Numerical experience showed that close to the stability limits of the dominating absorbers it is advantageous to prescribe the fraction f of the condensible material condensed in the dust and then using the corresponding P-T relations (like Eq. (18) for forsterite, for instance) simultaneously with the disk equations to solve for the radius s. This was done for $0.99 \geq f \geq 0$. In the remaining part of the intervals between the stability limits of two important absorbers the disk equations where solved for a sufficiently dense s-grid and iterating for the degree of condensation f of the dust species.

The opacity in the region between the annealing of the amorphous silicates and the destruction of aluminium compounds was calculated as

$$\kappa = f_{\rm Si} \cdot \kappa_{\rm olivine} + f_{\rm Fe} \cdot \kappa_{\rm iron} + f_{\rm Al} \cdot \kappa_{\rm corundum} \qquad (72)$$

where $f_{\rm Si}$ denotes the fraction of all Si condensed into enstatite and (or) forsterite, $f_{\rm Fe}$ the fraction of the iron condensed in iron grains and $f_{\rm Al}$ the fraction of aluminium condensed into the aluminium compounds. These fractions are calculated for the chemical equilibrium state. Strictly speaking, the Rosseland mean opacity of a mixture cannot be obtained by simply adding the Rosseland mean opacities of the individual components. Since (i) dust opacities are rather smooth and (ii) usually the opacity of one of the components strongly dominates the opacity of the mixture, Eq. (72) is nearly correct for such temperature and pressure conditions where the opacity is dominated by one component and can be taken as a smooth interpolation procedure in the transition regions.

The resulting P-T stratification in the midplane of the accretion disk is shown in Fig. 16. This curve shows four distinct temperature plateaus each corresponding to a strong reduction of the opacity related to the following processes:

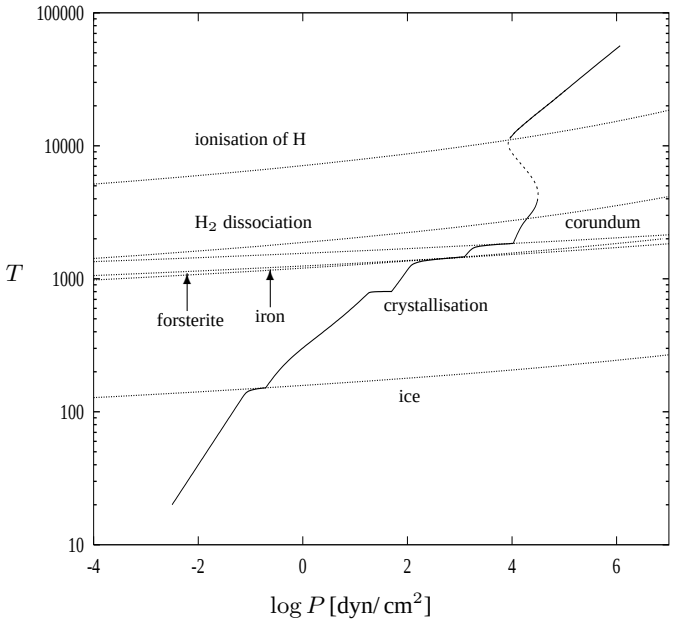

Fig. 16. Temperature-pressure stratification in the midplane of an accretion disc model with $M = 1 M_\odot$ and $\dot{\mathbf{M}} = 10^{-7}\, M_\odot/a$. The dotted lines show the limit lines for vapourisation of H_2O ice resp. decomposition and vapourisation of the indicated dust components and the limit lines for dissociation of H_2 and ionisation of H. The dashed part of the P-T stratification corresponds to the unstable branch of the solution in the region where multiple solutions of the stationary disk equations exist.

1. vapourisation of ice mantles on grains at about 150 K [5],
2. crystallisation of the dirty silicate dust inherited from the molecular cloud at about 800 K,
3. vapourisation of iron grains and chemisputtering of forsterite, which both occur at about 1 430 K, and
4. chemisputtering of corundum grains at about 1 840 K.

More precise limits are listed in Tab. 3 together with stability limits for some other dust components which are less important for the opacity.

The dashed part of the P-T stratification shown in Fig. 16 in the inner region of the disk corresponds to a multiple solution of the stationary disk equations which is due to the strong opacity increase with increasing temperature in the region of partial hydrogen ionisation. There exist two singular radii at $s = 0.1861$ AU and $s = 0.0727$ AU between which the disk equations have three different solutions of which only the lower and upper one are stable. Between the two singular radii there necessarily occurs a discontinuity in the disk structure where the solution jumps from the low temperature branch of the solution valid for the cold outer part of the accretion disk to the high temperature branch of the solution valid for the hot inner part of the accretion disk close to the star. This jump can occur at any point somewhere between the two singular points. Its position cannot be specified within the frame of the approximation of a

[5] The vapourization of ice mantles is not discussed in this paper, but it is included in the model programm.

Table 3. Stability limits according to chemical equilibrium calculations for some important solids in the protoplanetary disk.

solid	formation			disappearance		
	T [K]	P [dyn/ cm^2]	s [AU]	T [K]	P [dyn/ cm^2]	s [AU]
corundum	1541	$1.38\,10^{+3}$	0.221	1844	$1.05\,10^{+4}$	0.088
melilite	1459	$1.15\,10^{+3}$	0.256	1691	$9.58\,10^{+3}$	0.090
spinel	1016	$5.19\,10^{+2}$	0.320	1541	$1.38\,10^{+3}$	0.221
diopside				1464	$1.23\,10^{+3}$	0.231
anorthite				1019	$5.22\,10^{+2}$	0.318
iron				1462	$1.23\,10^{+3}$	0.231
forsterite				1428	$6.07\,10^{+2}$	0.321
enstatite				1319	$1.48\,10^{+2}$	0.617
amorphous silicate				803	$4.99\,10^{+1}$	0.922
troilite				719	$1.44\,10^{+1}$	1.626
ice mantle				151	$1.95\,10^{-1}$	8.693

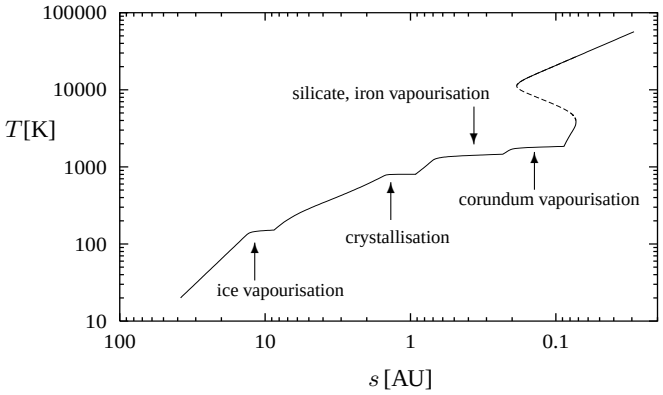

Fig. 17. Radial variation of the midplane temperature in a protoplanetary accretion disk model with $\dot{M} = 10^{-7} M_\odot / a$ and $M = 1 M_\odot$. The dashed part indicates the unstable branch of the solution in the region where multiple solutions of the stationary disk equations exist.

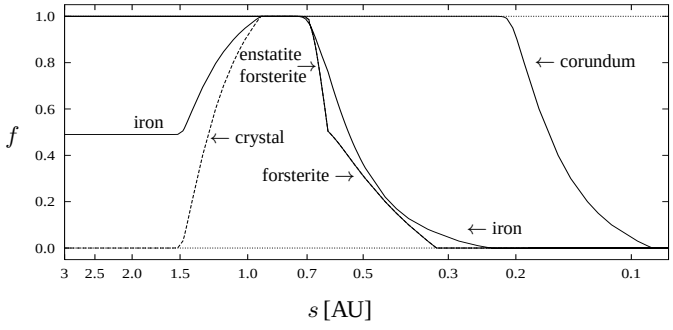

Fig. 18. Radial variation of the degree of condensation f for silicon in the silicates, of aluminium in corundum (and in some other aluminium compounds), and of iron in solid iron grains in the protoplanetary accretion disk model with $\dot{M} = 10^{-7} M_\odot / a$ and $M = 1 M_\odot$. The dashed line shows the degree of conversion of the initially amorphous silicate into crystalline silicate.

stationary disk. For time dependent models the discontinuity in the solution for the stationary model corresponds to wave fronts running to and fro in the region between the inner and outer singular points which in case of cataclysmic variables are the well known disk instabilities leading to the phenomenon of dwarf nova outbursts (see, e.g., the review by Cannizzo 1993). In the case of protoplanetary accretion disks this instability is thought to be responsible for the FU Ori outbursts (e.g., Hartmann & Kenyon 1996). Between the two singular radii of the stationary solution the disk temperature can either be low ($\lesssim 3\,500$ K) or high ($\gtrsim 10\,000$ K). Which of the two states is realised at a specific radius and instant depends on the history of the disk evolution and can only be determined from time dependent models. A simple test calculation following essentially the approximations described in Ruden & Pollak (1991) and Bell & Lin (1994) showed that for most of the time the jump occurs near the outer singular point and that only a few and short excursions to the inner singular point occur during the evolution of the disk. It is important to note that in the inner disk region between the two singular points the disk matter repeatedly switches two and fro between a hot state where the matter is ionised and a cold state where molecules easely form and some solid state species like corundum are stable.

Fig. 17 shows the radial distribution of the temperature. The plateaus corresponding to the disappearance of an important absorber can clearly be recognised. The plateau related to the transition from amorphous to crystalline silicate dust is quite extended between ≈ 1.5 AU and ≈ 0.92 AU. The variation of the fraction of crystallised material calculated from Eq. (70) is shown in Fig. 18. The drop in opacity associated with progressing crystallisation keeps the temperature in this region at a rather constant level of ≈ 800 K and spreads the whole transition across an extended radius interval. The temperature in this region between the present positions of Mars and Venus is much lower than what one would obtain if annealing is not considered. This unexpectedly low temperature in the region of terrestrial planets certainly has strong implications for the composition of planets to be formed in this region.

Once crystallisation has completed the midplane temperature in the disk rapidly increases to about 1 300 K between ≈ 0.92 AU and ≈ 0.65 AU and then slowly rises to ≈ 1460 K

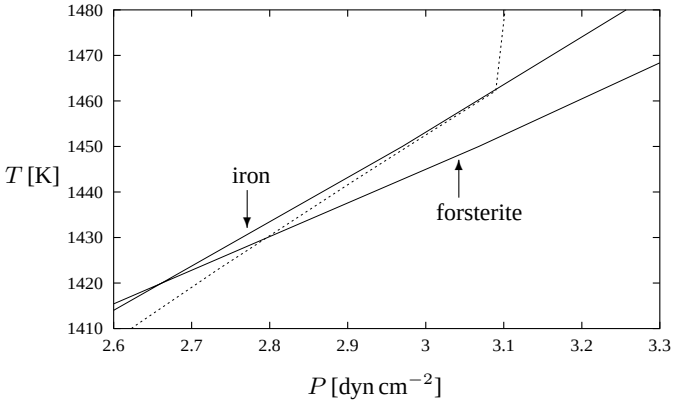

Fig. 19. Pressure and temperature in the midplane of the disk in the region of iron and silicate grain destruction (dashed line). The full lines show the stability limits of forsterite and iron.

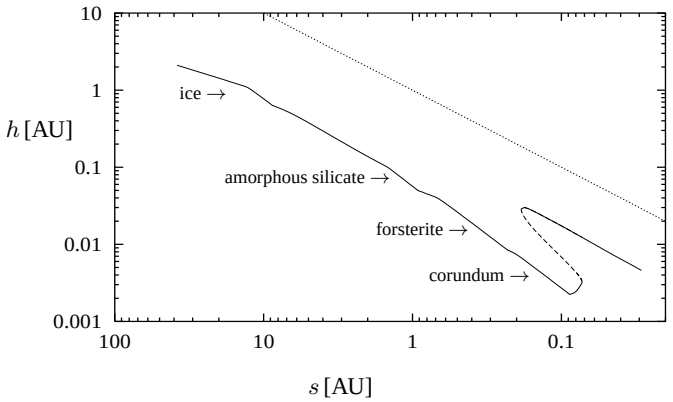

Fig. 20. Radial variation of the disk height h of a protoplanetary accretion disk model with $\dot{M} = 10^{-7} M_\odot/\,a$ and $M = 1 M_\odot$. The labels point to regions of strong opacity changes by disappearance of the indicated dust component. The dotted line corresponds to $h = s$.

between ≈ 0.65 AU and ≈ 0.23 AU when iron and olivine dust grains disappear. Both dust species disappear in the region in the P-T plane where their respective stability limit curves just intersect. The region of iron and silicate destruction is shown in more detail in Fig. 19. The pressure and temperature relation corresponding to the midplane of the disk crosses the limit lines for stability of iron and forsterite close to the point where both intersect. With our model parameters, the thermochemical data of Sharp & Huebner (1990), and with our assumptions with respect to the extinction coefficient the P-T relation first crosses the stability limit for forsterite and then the stability limit for iron. In our model there exists a region in the disk where iron exists as a solid but no silicates, a result which has already been found in other calculations (e.g. Grossman 1972, Lattimer et al. 1978) based on a somewhat different input physics for the structure of the solar nebula.

The destruction of iron and silicate grains is followed by a rapid rise of the temperature to approx 1 800 K and an extended temperature plateau until the last corundum grains are destroyed at $\approx$ 1840 K at a distance of only $s = 0.088$ AU from the star. Closer to the star the temperature rapidly increases in the region of molecular dominated opacity and with the onset of H^- absorption the solution jumps to the high temperature branch.

Fig. 17 shows that there is a considerable overlap in the radius of existence for the low and high temperature branch of the solution of the disk equations between $s = 0.1861$ AU and $s = 0.0727$ AU. This regime extends nearly over the whole radius regime where corundum grains do exist on the lower branch of the solution. On the high temperature branch the midplane temperature exceeds 10^4 K and neither molecules nor dust exist on this branch of the solution. Between $s = 0.1861$ AU and $s = 0.0727$ AU there exists no dust if the disk is in this high temperature state. If the instability of the disk solution in this regime is really related to the observed FU Ori outbursts then during the viscous stage of the disk evolution the corundum and other aluminium dust grains occasionally are formed in this region as the disk switches from the high temperature branch of the solution to the low temperature branch. The dust material vapourised

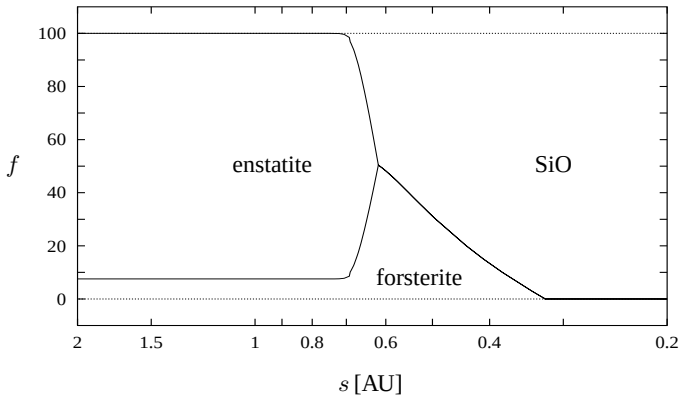

Fig. 21. Radial variation of the fraction of the silicon condensed into forsterite and enstatite and that remaining as SiO molecules in the gas phase. The ordinate is the percentage of the silicon bound in the solid.

during the hot phase then probably condenses again into new dust grains, either on newly formed condensation nuclei or on grains which survived in colder regions of the disk and which are mixed by transport processes (drift, turbulent diffusion) into the previously hot zone. In this region, the calcium-aluminium rich dust grains obviously are strongly modified in their properties and size and in their extinction properties due to this repeated "thermal treatment" which in turn modifies the disk structure. Such effects can only be treated on the basis of time dependent models for the disk evolution which are out of the scope of this paper.

Fig. 20 shows the radial variation of the disk height. The assumption of a "thin" disk upon which our disk equations are based is obviously satisfied. The solution shows an abrupt change in the disk height at the position of the jump from the low to the high temperature branch of the solution. The region of the disk adjacent to this hump is shadowed from direct insolation from the protosun.

Fig. 21 shows the result for the radial variation of the abundance of enstatite and forsterite dust in the disk according to

chemical equilibrium. Minor silicon bearing dust components are neglected in this figure. Most of the silicon forms enstatite and only in a small zone in the inner part of the protoplanetary disk the forsterite is the dominating silicate dust component. The equilibrium mixture of enstatite and forsterite is different from the mixture assumed in the P94 dust model to enter the accretion disk from the parent molecular cloud. Considerable internal diffusion and restructuring processes are required to convert the dust mixture from the molecular cloud core into a mixture corresponding to a chemical equilibrium state. Whether this conversion is possible is an important question for the structure of the inner parts of the protoplanetary accretion disk which requires further detailed studies of the basic chemical and physical processes in a protoplanetary accretion disk.

9. Concluding remarks

In this paper we have considered the various dust components present in a protoplanetary accretion disk. We have seen that the initial mixture of grains entering the disk from the parent molecular cloud, as given for instance by the P94 model, does not correspond to the mixture of solids which one encounters in a chemical equilibrium state for a Solar System element mixture. As the disk material slowly spirals inwards during the viscous evolution of the accretion disk the material gradually becomes hotter. This activates previously kinetically forbidden local rearrangement processes within the grain lattice and solid diffusion in the grain material. As a result of such processes a considerable change of the structural properties and of the chemical composition of the dust component in the protostellar accretion disk can be expected to occur in the warm inner parts of the accretion disk. The annealing of the initially amorphous lattice structure of dust grains and chemical fractionation processes strongly modify the extinction properties of the dust component of the disk material which in turn strongly modifies the radial temperature structure of the accretion disk. A realistic modelling of the structure and evolution of protoplanetary accretion disks, thus, requires a detailed consideration of the chemical transmutation of the dust material during the accretion process. The present paper is a first attempt to figure out what type of processes may be important in this connection and what are the consequences of such processes for the disk structure.

The calculations with respect to the possible condensates in a chemical equilibrium state to some extent repeats earlier calculations on condensation sequences for the Solar Nebula (e.g. Grossman 1972, Lattimer et al. 1978, Saxena & Eriksson 1986, Sharp & Huebner 1990). Though it seems now clear that the type of processes envisaged by the early calculations – condensation of solids from the gas phase in a contracting cooling nebula – is not the process really operating in a protoplanetary disk the predictions for the appearance and disappearance of certain minerals at certain temperatures does not depend critically on the assumptions with respect to the structure of the object. While most of the earlier calculations are performed for only one or a few fixed values of the pressure, the method used in this paper of constructing curves for a given degree of condensation has the advantage of showing clearly the region of existence of the various dust materials in a wide region of the pressure and temperature plane. The results therefore give a broader insight into which dust material may be important under varying pressure-temperature conditions in the protoplanetary accretion disk.

A major shortcoming of the type of equilibrium calculations based on the methods of chemical thermodynamics as have been performed in the present paper and in all earlier paper on condensation sequences is that in a real accretion disk the evolution of the chemical system into the chemical equilibrium state may be hindered either by activation energy barriers or by the slowness of the solid state diffusion processes required if certain atomic species have to be transported from the gas phase into the interior of a grain or have to be driven out of the grain during the conversion from one condensate to another one at the border of stability between the two compounds. A more realistic treatment of the chemical transmutation of the dust components in a protoplanetary disk requires a much more detailed treatment of the transport processes within the grains as it was possible to perform in the present paper. Additionally a kinetical treatment of the chemical surface reactions during growth or destruction of the different dust components is required but presently this is not possible since the details of the individual reaction steps are not known. Further progress in the understanding of the structure and evolution of the inner parts of a protoplanetary system requires further efforts with respect to clarifying which are the basic processes responsible for the chemical evolution of the dust component.

In our calculations we did not account for radial mixing due to turbulent motions which inevitably occurs during the viscous evolution of the disk (e.g. Morfill et al. 1985, Stevenson & Lunine 1988). This process intermingles material from different zones of the disk or accumulates material in the vaporization-condensation zone of solids and the rather simple radial distribution of different dust materials obtained in the present calculation would become more complicated instead. Since mixing occurs on timescales comparable to the evolutionary timescale of the disk such effects can only be treated within the frame of time dependent calculations of the disk evolution.

Acknowledgements. This work has been supported by the Deutsche Forschungsgemeinschaft (DFG), Sonderforschungsbereich 359 “Reaktive Strömungen, Diffusion und Transport”.

References

Atkins P.W., 1994, Physical Chemistry, 5th Ed., Oxford University Press, Qxford etc.

Anders E., Grevesse N., 1989, Geochimica et Cosmochimica Acta 53, 197

Ashworth J.R., Mallinson L.G., Hutchinson R., Biggar G.M., 1984, Nat 308, 259

Bell K.R., Lin D.N.C., 1994, ApJ 427, 987

Bradley J.P., 1994, Sci 265, 925

Cannizzo J.K., 1993, In: Wheeler J.C. (ed.) Accretion disks in compact stellar systems, World Scientific Publ. Comp., Singapore etc., p. 6

Cassen P., 1994, Icarus 112, 405
Dekker A.J., 1963, Solid State Physics, Macmillan, London
Duschl W.J., Gail H.-P., Tscharnuter W.M., 1996, A&A 312, 624
Dorschner J., Henning T., 1995, A&AR 6, 271
Dorschner J., Begemann B., Henning Th., Jäger C., Mutschke H., 1995, A&A 300, 503
Draine B.T., 1985, ApJS 57, 587
Draine B.T., Lee H.M., 1984, ApJ 285, 89
Fegley Jr. B., Prinn R.G., 1989, In: Weaver H.A., Danly L. (eds.) The Formation and Evolution of Planetary Systems, Cambridge University Press, Cambridge, p. 171
Finocchi F., Gail H.-P., Duschl W., 1997, A&A 325, 1264
Finocchi F., Gail H.-P., 1998, *in preparation*
Gail H.-P., Sedlmayr E., 1998, In: Hartquist T.W., Williams D.A. (eds.) The Molecular Astrophysics of Stars and Galaxies, Oxford University Press (in press)
Goodman A.A., Whittet D.C.B., 1995, ApJ 455, L181
Grevesse N., Noels A., 1993, In: Prantzos N., Vangioni-Flam E., Cassé M. (eds.) Origin and Evolution of the Elements, Cambridge University Press, Cambridge, p. 15
Grossman L., 1972, Geochimica et Cosmochimica Acta 36, 597
Hartmann L., Kenyon S.J., 1996, ARA&A 34, 207
Huffman D.R., Stapp J.L., 1973, In: Greenberg J.M., van de Hulst H.C. (eds.) Interstellar Dust and Related Topics, Proc. IAU Symp. 52, Reidel, p. 297
Huss G.R., Fahey A.J., Gallino R., Wasserburg G.J., 1994, ApJ 430, L81
Hutcheon I.D., Huss G.R., Fahey A.J., Wasserburg G.J., 1994, ApJ 425, L97
Koike C., Kaito C., Yamamoto T., Shibai H., Kimura S., Suto H., 1995, Icarus 114, 203
Kuskov O.L., Galimzyanov R.F., 1986, In: Saxena S.K. (ed.) Chemistry and Physics of Terrestrial Planets, Springer, New York etc., p. 310
Lattimer J.M. , Schramm D.N., Grossman L., 1978, ApJ 219, 230
Lauretta D.S., Kremser D.T., Fegley Jr. B., 1996, Icarus 122, 288
Lenzuni P., Gail H.-P., Henning Th., 1995, ApJ 447, 848
Li A., Greenberg J.M., 1997, A&A 323, 566
Lide R.D., 1995, CRC Handbook of Chemistry and Physics, 76th ed., CRC Press, Boca Raton etc.
Lunine J.I., Engel S., Rizk B., Horanyi M., 1991, Icarus 94, 333
Martin P.G., 1995, ApJ 445, L63
Mathis J. S., Rumpl W., Nordsieck K. H., 1977, ApJ 217, 425
Mathis J.S., 1996, ApJ 472, 643
Miyake K., Nakagawa Y., 1993, Icarus 106, 20
Morfill G.E., Tscharnuter W., Völk H.J., 1985, In: Black D.C., Matthews M.S. (eds.) Protostars and Planets II, University of Arizona Press, Tucson, p. 493
Neufeld D.A., Hollenbach D.J., 1994, ApJ 428, 170
Nittler L.R., Alexander C.M., Gao X., Walker R.M., Zinner E.K., 1994, Nat 370, 443
Nuth J.A., Donn B., 1982, ApJ 257, L103
Pollack J.B., Hollenbach D., Beckwith S., Simonelli D.P., Roush T., Fong, W., 1994, ApJ 421, 615
Prinn R.G., Fegley Jr. B., 1989, In: Atreya S.K., Pollak J.B., Mathews M.S. (eds.) Origin and Evolution of Planetary and Satellite Atmospheres, University of Arizona Press, Tucson, p. 78
Rietmeijer F.J.M., Mackinnon I.D.R., 1985, Nat 315, 733
Ruden S.P., Pollack J.B., 1991, ApJ 375, 740
Ruzmaikina T.V., Ip W.H., 1994, Icarus 112, 430
Saxena S.K., Eriksson G., 1983, Geochimica et Cosmochimica Acta 47, 1865
Saxena S.K., Eriksson G., 1986, In: Saxena S. K. (ed.) Chemistry and Physics of Terrestrial Planets, Springer, New York etc., p. 30
Sears D.W.G., Dodd R.T., In: Kerridge J.F., Matthews M.S. (eds.) Meteorites and the Early Solar System, University of Arizona Press, Tucson, p. 3
Sharp C.M., Huebner W.F., 1990, ApJS 72, 417
Stahler S.W., 1983, ApJ 274, 822
Stevenson D.J., Lunine J., 1988, Icarus 75, 146
Stognienko R., Henning Th., Ossenkopf V., 1995, A&A 296, 797
Weast, R.C., Astle, M.J., 1981, CRC Handbook of Chemistry and Physics, CRC press, Boca Raton
Willis J., Goldstein J.I., 1981, Nat 293, 126